PAPER

Lysozyme activated co-delivery of latanoprost–timolol from mucoadhesive chitosan nanocomposite to manage glaucoma†

B. N. Kumara, [ID] [a] R. Shambhu,[b] Yoon-Bo Shim [ID] [c] and K. Sudhakara Prasad [ID] *[a,d]

Glaucoma is a leading cause of irreversible blindness, and controlling intraocular pressure is imperative for good clinical outcomes. It is important to use natural stimuli to trigger the release of the drug when it is linked to a nanoparticle/nanocomposite, particularly in ophthalmic applications to maintain sustained release. Herein the preparation and investigation of biocompatible, mucoadhesive dual drug-loaded chitosan (CS)–graphene quantum dot (GQD) nanocomposites are reported. Drug release from the nanocomposite was controlled by the presence of a natural lacrimal fluid enzyme, lysozyme (Lyz). Lyz is efficient at cleaving the β-1,4 glycosidic linkages of CS, thereby releasing the drug of interest. A biocompatible, fluorescent nanomaterial *i.e.*, GQDs, was employed to track drug loading by using simple photoluminescent spectral studies. The optimized nanocomposite encapsulation efficiencies (EEs) were 94.51% and 74.08% for latanoprost (LP) and timolol (TM) and delivered 32.68% and 66.61% of drugs, respectively, in 72 h. Dual drug delivery through the cleavage of β-1,4 glycosidic linkages of CS in the presence of Lyz was confirmed through ^{1}H-NMR and FE-SEM studies. An increase in the particle size from 490 nm to 1584 nm in the presence of mucin supports the mucoadhesiveness of the nanocomposite. The *in vitro* cytocompatibility and live/dead staining assays against human corneal epithelial (HCE) cells showed ≥80% cell viability. *Ex vivo* tests proved that the nanocomposite was non-irritant, and histopathological studies showed normal growth of blood vessels. Molecular docking studies showed the hydrogen bonding and electrostatic interactions between the drug and CS. Hence the developed nanocomposite could be used as an ocular suspension or nanocomposite for further preclinical studies on glaucoma management.

1. Introduction

Glaucoma is a neurodegenerative disorder that leads to blindness if untreated.[1,2] In addition, progressive loss of retinal ganglion cells due to increased intraocular pressure (IOP) could occur. Mainly, there are two kinds of glaucoma, open-angle glaucoma (OAG) and angle-closure glaucoma (ACG). OAG is a slow progressive atrophy of the optic nerve, characterized by a loss of peripheral visual function, whereas ACG is caused by sudden pain followed by blurred vision.[3] However, in both cases, typical symptoms are cupping and atrophy of the optic nerve head, visual imbalance, and increased IOP.[4] The main cause of glaucoma is the elevation of IOP in the eye. To manage glaucoma, several medications are available on the market in the form of eye drops[5] and ocular suspensions.[6] Some of the commercial formulations are, individual and combinations of prostaglandin analogues, β-blockers, α-2 agonists, carbonic anhydrase inhibitors, and muscarinic receptor agonists.[7] Among these, prostaglandin analogues and β-blockers are found to be effective at managing glaucoma.[8–10] When it comes to the mechanism of action, these prostaglandin analogues suppress IOP by initiating aqueous humor drainage through the uveoscleral outflow pathway whereas β-blockers bind to β1 and/or β2 receptors in the ciliary body to decrease the production of aqueous humor.[4] However, these formulations are not effective as eye drops or ocular suspensions due to the continuous loss of drugs during periodic eye blinks followed by rapid lacrimal fluid outflow. Numerous studies suggest that only 1–5% of the administered drug is absorbed in the corneal region due to a short residence time, whereas

[a]*Nanomaterial Research Laboratory (NMRL), Nano Division, Yenepoya Research Centre, Yenepoya (Deemed to be University), Deralakatte, Mangalore 575 018, India. E-mail: ksprasadnair@yenepoya.edu.in; Fax: +91-824220 4667; Tel: +91-824 220 4668-2035*

[b]*Department of Ophthalmology, Yenepoya Medical College, Yenepoya (Deemed to be University), Deralakatte, Mangalore 575 018, India*

[c]*Department of Chemistry, Institute of BioPhysio Sensor Technology (IBST), Pusan National University, Busan 46241, South Korea*

[d]*Centre for Nutrition Studies, Yenepoya (Deemed to be University), Deralakatte, Mangalore 575 018, India*

†Electronic supplementary information (ESI) available. See DOI: https://doi.org/10.1039/d4pm00031e

the remaining medication is flushed out with lacrimal fluid outflow resulting in low bioavailability of the drug at the cornea.[11–13] Hence, mucoadhesive polymers could be employed for the production of ocular suspensions or eye drops.[14]

Recently, efforts have been made to develop dual anti-glaucoma drug (prostaglandin analogue & β-blocker) loaded nanocomposites to synergistically tackle glaucoma by reducing IOP. In addition to this, elevating the mucoadhesiveness of the nanocomposite to improve the long-term delivery of the therapeutic payload at the cornea has also been explored. Latanoprost (LP) and timolol (TM) loaded CS and alginate nanosheets prepared *via* a spin coating method showed variable degrees of drug release (25, 82, and 95%) for up to 48 h resulting in uncontrolled drug delivery and a lack of mucoadhesiveness.[15] The LP and TM loaded poly(ethylene glycol) methyl ether–polylactic acid (mPEG–PLA) micelles showed an initial burst release of 0.70 μg of LP and 57.12 μg of TM, and no drugs were found after 24 h. A contact lens made from the same material showed excellent results when compared with eye drops and showed an impressive decrease in IOP;[8] however, the *in vitro–in vivo* correlations (IVIVC) are poor because the *in vivo* release rates are lower than the *in vitro* values.[16] Hence, by considering the lack of controlled delivery, stimuli responsiveness, and the absence of drug in the long term, there is a need to develop highly mucoadhesive, long-term dual-drug deliverable nanocomposites for glaucoma treatment.

A plethora of polymers have been reported for the preparation of hydrogels and nano-formulations by using biocompatible polymers such as sodium alginate, chitosan (CS), gellan, carrageenan, and Carbopol.[17] Among these, CS is found to be a versatile material due to its biocompatible, biodegradable, highly mucoadhesive, and polycationic properties with a capacity to entrap the drug of interest, and most importantly the quality of undergoing degradation in the presence of lysozyme (Lyz).[18–22] Lyz is a protein, abundantly available in human lacrimal fluid, saliva, human milk, and pig sow milk.[23] Interestingly, CS undergoes degradation through the breaking of β-1,4 glycosidic linkages in the presence of Lyz, chitinases, and proteases. Notably, several chromogenic agents and organic dyes are utilized in implants or nanocomposites to confirm drug loading and delivery such as fluorescein isothiocyanate (FITC) and sodium fluorescein (NaF) dyes, questioning the biocompatibility of the developed materials.[24–27]

To overcome this bottleneck, biocompatible fluorescent nanomaterials could be a better option.[28] In particular, graphene quantum dots (GQDs) are non-cytotoxic, photoluminescent, biocompatible, and aqueous soluble materials having sizes ranging from 2 to 10 nm.[29] With its unique photoluminescence (PL) properties, GQD has been extensively explored for bioimaging and drug delivery applications.[30–32] With tracking evidence from proof-of-concept studies,[32] in the present work, we employed GQDs for dual drug loading confirmation by emission spectra, band gap, and fluorescence lifetime studies.

Taken together, with the unique properties of CS and GQD, and considering the present drawbacks of dual drug delivery platforms for glaucoma management, herein we fabricated biocompatible, highly mucoadhesive, hydrophobic (LP), and hydrophilic (TM) drug-loaded CS nanocomposites, which could deliver the drug through the cleavage of the β-1,4 glycosidic bonds of CS in the presence of Lyz available in lacrimal fluid. The newly synthesized dual drug-loaded nanocomposite not only assured sustained delivery in the long term without burst release but also facilitated excellent biocompatibility with non-irritant characteristics. Notably, the present work opens an avenue for the simultaneous release of LP and TM for 72 h to treat glaucoma by utilizing a naturally secreting enzyme, Lyz. We believe that the developed platform is promising as a composite material for the production of contact lenses that can deliver the dual drug to arrest the rapid diffusion of the drugs as well as prevent overdose side effects.

2. Materials and methods

2.1. Materials

Chemicals such as graphene oxide (GO, 2 mg mL^{-1}), latanoprost (LP), timolol maleate salt (TM), sulfuric acid (H$_2$SO$_4$), branched polyethyleneimine (PEI, average $M_w \sim 800$ by LS, average $M_n \sim 600$ by GPC), succinic acid (SA), 1-ethyl-3-[3-dimethylamino propyl]-carbodiimide hydrochloride (EDC), *N*-hydroxy succinimide (NHS), chitosan (CS, MW: 50 000–190 000 Da, based on viscosity), lysozyme (Lyz, ≥40 000 units per mg protein) from egg white, 3-(4,5-dimethylthiazol-2-yl)-2,5-diphenyl-2*H*-tetrazolium bromide (MTT), acridine orange (AO), acetic acid, ethidium bromide (EB), and dimethyl sulfoxide (DMSO) were obtained from Sigma-Aldrich Chemicals Pvt. Ltd, Bangalore, India. Furthermore, we procured hydrochloric acid (HCl), isopropyl alcohol, sodium chloride (NaCl), sodium bicarbonate (NaHCO$_3$), potassium chloride (KCl), calcium chloride dihydrate (CaCl$_2$·2H$_2$O), mucin (from the porcine stomach, type II, bound sialic acid, ≤1.2%), sodium hydroxide (NaOH), formaldehyde solution (37%), and deuterium oxide (D$_2$O) from Merck Specialties Pvt. Ltd, Bangalore, India, and nitric acid (HNO$_3$) from HiMedia Laboratories Pvt. Ltd, Mumbai, India. The procured chemicals were used as received without any further purification. The cell culture reagents were obtained from Thermo Fisher Scientific Ltd, Gibco, Bangalore, India.

2.2. Instrumentation

To study the optical properties by UV-visible spectroscopy (UV-Vis), a UV-1800 Shimadzu UV spectrophotometer, Japan, was used, emission spectroscopy experiments were performed by employing an F-2700 FL spectrophotometer and fluorescence lifetime measurements were performed using a Jobin Yvon Fluorolog-3-11 spectrofluorimeter (450 W xenon lamp). Furthermore, Fourier transform-infrared spectroscopic investigations were performed with an attenuated total reflectance mode (FTIR-ATR, Shimadzu, Kyoto, Japan) instrument. Surface

morphological studies of the nanocomposite were analyzed by using high resolution-transmission electron microscopy (HR-TEM, JEOL Ltd, Tokyo, Japan) and field emission-scanning electron microscopy (FE-SEM, Carl Zeiss, Germany) instruments. The particle size and zeta potential analyses of the prepared dual drug-loaded nanocomposites were performed by using a Malvern Zetasizer Ultra instrument. *In vitro* biological studies were performed by using ZOE, BioRad, and a microplate reader (FluoSTAR Omega, BMG Labtech) instrument. To quantify the TM and LP contents, a Shimadzu Prominence ISO LC series HPLC instrument at 254 nm and 210 nm (Thermo Scientific™ Hypersil™ ODS C18 column, 5 μ, 300 × 4.6 mm) was employed. Furthermore, chemical characterization studies were performed by ^{1}H-NMR (500 MHz, 298 K) on a Bruker ASCEND™ spectrometer. To capture the images of the HET-CAM assay, an android mobile phone was used. For the histopathological examination and imaging, a microtome instrument and fluorescence microscope were employed.

2.3. Preparation of dual drug-loaded CS–GQD nanocomposite

To prepare the dual drug-loaded CS–GQD nanocomposite (drug nanocomposite), GQD was synthesized as per a previous method by using graphene oxide (GO) as a precursor in the presence of a 1 : 3 ratio of sulphuric acid (H_2SO_4) and nitric acid (HNO_3) at 120 °C for 24 h. Furthermore, surface passivation was performed as reported.[32]

Before the addition of the dual drug to CS, the required amounts of LP (LP, 30 μg) and TM (TM, 600 μg) were mixed and stirred for a few minutes. In brief, 75–85% deacetylated CS was mixed with the dual drugs (LP and TM) followed by addition to a prepared passivated GQD in the presence of a 1 : 3 ratio of EDC/NHS (1 mg/250 μL) to create the drug nanocomposite. Low molecular weight (LMW) CS (2, 3, 5, and 7% w/v) was dissolved in deionized water containing 2% (v/v) acetic acid and stirred overnight at 1500 rpm. The CS gel was sonicated for 5 min to remove bubbles. To the obtained CS gel, 2 M NaOH was added to adjust the pH from 3.3 to 5.5, making it slightly acidic for enhanced drug loading. After the successful preparation of the dual drug nanocomposite, the pH was adjusted to 7.4. Subsequently, the resulting drug nanocomposite was dialyzed in simulated lacriaml fluid (pH: 7.4) for a few hours with 0.5–1 kDa MWCO membrane (Spectrum Labs) to remove unbound LP and TM and excess unreacted EDC/NHS. Quantification of the unbound drug was achieved by using HPLC at wavelengths of 210 nm and 254 nm. The resulting final nanocomposite was stored in the refrigerator for further use.

To maintain the sterility of the developed drug nanocomposite, before using the materials for the preparation, they were filtered using 0.22 μm and 0.45 μm syringe filters under sterile conditions followed by dialysis using 0.5–1 kDa membrane. Furthermore, the developed drug nanocomposite was exposed to UV radiation of 100–280 nm in wavelength before

the *in vitro* cell culture studies and HET-CAM analysis were conducted.[33]

2.4. Entrapment efficiency and loading capacity

The entrapment efficiency (EE) and loading capacity (LC) of combinatorial drugs, namely, LP and TM, were determined by HPLC analysis at 210 nm and 254 nm. The below-mentioned formulas were used to calculate both EE and LC.[34]

$$EE(\%) = [(\text{total amount of Drug} - \text{free Drug in the supernatant}) / \text{total amount of Drug}] \times 100 \quad (1)$$

$$LC(\%) = [\text{total amount of drug} / \text{total amount of nanocomposite}] \times 100 \quad (2)$$

2.5. *In vitro* dual drug release studies

To study *in vitro* drug release from the nanocomposite, different concentrations of Lyz (300, 600, 1000 μg mL^{-1})-treated drug nanocomposites (2 mL) were loaded into a 0.5–1 kDa molecular weight cutoff membrane (MWCM), which was then placed in a beaker containing STF (pH 7.4) at 37 °C under medium stirring to maintain the physiological conditions. Besides, 1 mL of the released medium was collected from the beaker at pre-determined time points, namely, 1, 6, 12, 24, 36, 48, and 72 h, and replenished with the same amount of STF to maintain a constant sink volume. The collected samples were stored in a −20 °C refrigerator until the analysis. Furthermore, collected samples were simultaneously quantified by HPLC analysis. The drug release experiments were performed in triplicate ($n = 3$).

The mathematical modelling of the obtained drug release data was performed by using Kinet_DS (version 3.0) and DDSolver®. The *in vitro* drug release data fit to various standard kinetic equations, namely, zero-order, first-order, Korsmeyer–Peppas, and Hixson–Crowell models.[31] The selection of the model suggesting the drug release pattern from the dual drug-loaded nanocomposite was identified by considering the coefficient of regression (R^2) obtained from the models.

2.6. *In vitro* mucoadhesion studies

For mucoadhesive studies, the mucin–nanoparticle was used to investigate the mucoadhesive property of the formulation by considering the changes to the particle size. The procedure was followed as per previous reports.[31,35,36] The variation in particle size was analyzed by incubating the dual drug-loaded nanocomposite with mucin suspension (35 °C, 1% m/v). Before this, commercially available mucin was hydrated in demineralized water at 4 °C for 12 h. Furthermore, the mucin solution was diluted with 0.1 M PBS and the pH (7.4) was adjusted with 1 M NaOH. The prepared solution was ultrasonicated for 1 h to reduce the size followed by centrifugation at 4000 rpm for 20 min. The resulting supernatant solution was

filtered using a 0.45 μm filter membrane. The particle size of mucin was analyzed before conducting the study and only mucin smaller than 500 nm was considered for the investigation. Furthermore, to check the particle size variation upon mucin addition, equal volumes of drug nanocomposite and mucin particle suspension were mixed by vortexing for a minute and the obtained mixture was analyzed by the DLS technique.

2.7. ^{1}H-nuclear magnetic resonance (^{1}H-NMR) characterization of nanocomposites

The ^{1}H-nuclear magnetic resonance spectra (^{1}H-NMR) were recorded to determine the formation of hydroxyl groups due to the cleavage of β-1,4 glycosidic linkages of CS upon treatment with Lyz. To check the same, the dual drug-loaded nanocomposite (drug nanocomposite), degraded nanocomposite (dialysate), and Lyz-dual drug-loaded nanocomposite (retentate) were collected, freeze-dried, and re-dissolved in D$_2$O (0.5 mL per 20 mg) for analysis. Furthermore, the chemical structure was characterized by ^{1}H-NMR (500 MHz, 298 K) on a Bruker ASCEND^{TM} spectrometer.

2.8. Biological studies

To test the prepared nanocomposites *in vitro*, human corneal epithelial (HCE) cells were chosen. The HCE cells were cultured in Dulbecco's modified Eagle's medium (DMEM): Ham's F12 supplemented with 10% fetal bovine serum (FBS) and 1% antibiotic–antimycotic solution. The cells were incubated at 37 °C under 5% CO$_2$, subcultured upon attaining 70–80% confluence, and used for the experiments after three consecutive passages.

2.8.1. Cell viability assessment using methyl thiazolyl tetrazolium (MTT) assay. The cytotoxicity assay (MTT) was performed to assess the biocompatibility of the as-prepared nanocomposites with cultured HCE cells.[37] In 96 microtiter well plates, cells were seeded at a density of 5000 cells per well and incubated for 24 h at 37 °C under a humidified atmosphere with 5% CO$_2$. The untreated cells were used as a control. The drug nanocomposite and Lyz-treated drug nanocomposite were added to cells at concentrations of 20, 40, 60, 80, and 100 μg mL^{-1}, and the cells were incubated for another 24 h. Following incubation, spent media were removed from each well, and 100 μL of MTT solution with a concentration of 1 mg mL^{-1} was added to the wells and further incubated for 4 h. The absorbance of formazan crystals was measured at 570 nm using a multimode microplate reader after they were solubilized in 100 μL of DMSO. Furthermore, the cell viability percentage was calculated using the below-mentioned formula.

$$\text{Cell viability}(\%) = \frac{\text{optical density of cells treated with samples}}{\text{optical density of the control}} \times 100 \tag{3}$$

2.8.2. *In vitro* cell morphology studies. To assess the *in vitro* HCE cell morphology, different concentrations (20, 60,

and 100 μg mL^{-1}) of drug nanocomposite and Lyz-treated drug nanocomposite were used. For the analysis, cells were seeded at a seeding density of 10 000 cells per well in the 24-well plate followed by incubation at 37 °C under a humidified atmosphere with 5% CO$_2$ for 24 h. After 24 h, composites were treated at 20, 60, and 100 μg mL^{-1}. Upon the completion of 24 h of incubation, cell morphological images were captured using an inverted microscope (Zeiss). For the analysis of both test compounds, the control is prepared in the same way.

2.8.3. Acridine orange/ethidium bromide (AO/EB) staining assay. The AO/EB analysis is typically performed to assess the viable and apoptotic stages of cultured HCE cells.[38] For the experiment, HCE cells were seeded in 24 well plates at a seeding density of 10 000 cells per well and incubated at 37 °C under a humidified atmosphere with 5% CO$_2$ for 24 h. The test compounds, namely, drug nanocomposite and Lyz-treated drug nanocomposites, were added to the cells at various concentrations, 20, 60, and 100 μg mL^{-1}, and incubated for 24 h. After the required treatment period, spent media from the wells were removed and cells were washed with 1× PBS. Staining was carried out using AO/EB (2 μg mL^{-1}, 1 : 1) for 15 min at 37 °C under dark conditions. Excess stain was removed, and cells were again washed with PBS. Furthermore, cells were overlaid with PBS and imaged under green and red channels of a fluorescence imager. Nuclei with green fluorescence were regarded as viable, and cells with greenish-yellow or red fluorescence were regarded as apoptotic cells under the merge channel. For the analysis of both test compounds, the control is prepared in the same way.

2.9. Ocular tolerance test (HET-CAM test)

The ocular tolerability of the prepared formulation was studied by using a hen's egg test-chorioallantoic membrane (HET-CAM) assay. It is a well-known conjunctival model to explore the potential of an exterior irritant agent.[39] Furthermore, the irritant ability of the prepared compounds can be observed by the periodic changes to the chorioallantoic membrane of the egg upon exposure to the prepared materials/formulations. To evaluate the ocular tolerance, freshly fertilized eggs were incubated at 37 ± 0.5 °C for about 9 days. Next, the eggs were tested with a cold lamp to ensure the viability and optimal illumination of the chorioallantoic membrane followed by the observation of the development of an embryo. On the 10th day of incubation, the shells of the egg were scratched off around the air bubble using forceps. Furthermore, the inner membrane was moistened with saline solution, warmed to 37 °C, and carefully removed without injuring any underlying blood vessels to expose the CAM. Next, the prepared materials (300 μL) were applied to the surface of the CAM. In brief, the test materials, namely, GQD, GQD–PEI–SA (passivated GQD), CS, LP, TM, LP loaded nanocomposite, and the drug nanocomposite, as well as controls (control, positive and negative), were exposed to CAM. Notably, we have not tested Lyz on CAM, since Lyz is naturally available in lacrimal fluid. Each concentration was tested in triplicate and the mean scores were analyzed by considering the irritation. The test

compounds' activity was investigated over 5 min (at 1 min, 3 min, and 5 min) and photographs were taken at each time point. For this assay, 0.1 M sodium hydroxide (NaOH) solution was used as the positive control, saline (0.9% NaCl) solution was considered a negative control, and one group was left untreated (control). Furthermore, the irritant tolerability of blood vessels determined by hyperemia, haemorrhage, or coagulation was examined using a stereomicroscope.[40–42]

$$\text{Irritation score(IS)} = (301\text{-}h)/300 \times 5 + (301\text{-}l) /300 \times 7 + (301\text{-}c)/300 \times 9 \quad (4)$$

Here, 'h' refers to a time in seconds when a haemorrhage appears, 'l' is the time in seconds when lysis appears, and 'c' is considered as the time in seconds when coagulation is raised. The scores for non-irritants are considered to be 0–0.9, 1–4.9 are considered slight irritants, 5–8.9 are moderate irritants, and 9–21 are taken as severe irritants.

2.9.1. Histopathological studies. The control and treated CAM blood vessels were removed from the egg soon after the HET-CAM analysis (after 5 min) and stored in a 4% formalin solution for 24 h. The tissues were processed at different concentrations of ethanol and finally embedded in paraffin. Sections of the CAM tissues were sliced using a microtome and they were processed for hematoxylin and eosin (H&E) staining. The stained slides were scanned using the fluorescence microscope to check the structure of the primary, secondary, and tertiary capillaries.

2.10. Molecular docking

Molecular docking studies were performed to examine the interactions between the drug and the polymer.[43,44] Primarily, we investigated the possible interactions of CS and LP, followed by CS and TM. In addition, to understand the binding affinity between the dual drugs, the interactions between TM and LP were checked. For the analysis, structures were obtained from the PubChem database (chitosan (CS): 71853; latanoprost (LP): 5311221; timolol (TM): 5281056) and were prepared using MGL tools 1.5.6 followed by converting the results into PDBQT file format for input in AutoDock Vina 1.5.6. The drug and polymer were adjusted for the lack of hydrogen atoms and chirality with the stereo concoction and shape optimizations. AutoDock Vina 1.5.6 was used to carry out the docking studies and further calculations. The polymer and drug were docked to explore the possible binding affinity and interactions between them using the Discovery Studio 2021 Client software.

2.11. Statistical analysis

The plotted values of cytotoxicity and bright field imaging assays were calculated by taking mean ± standard deviation (n = 3). Statistical analysis was carried out using a one-way ANOVA analysis of variance A (Tukey's multiple comparison test) using GraphPad Prism 8 software. Statistical significance was assumed for p-values: ns = non-significant, *P < 0.05, **P < 0.01, ***P < 0.001, and ****P < 0.0001.

3. Results

Herein, we discuss the preparation and application of a dual drug-loaded nanocomposite (drug nanocomposite) for glaucoma management. Currently, many combination drugs are available on the market to reduce IOP; however, due to the frequent instillation of eye drops followed by rapid tear secretion, patients have trouble adhering to the existing treatment. Therefore, the present work investigates the delivery response of the drug nanocomposite in the presence of Lyz, wherein the drug, TM, is a β-adrenergic agent, and LP prostaglandin analogues were also employed. By considering that the natural enzyme present in lacrimal fluid has the ability to hydrolyze CS, we have examined the delivery response of nanocomposites in the presence of various concentrations of Lyz as shown in Scheme 1.

3.1. Preparation and characterization

We have formulated different compositions by varying the percentage of CS and without altering any other co-existing materials (section 2.3) and drugs as shown in Table 1. It should be noted that, for ocular drug delivery applications, the formulations should be highly transparent for better patient compliance. The formulations contain 2, 3, 5, and 7% of CS, and importantly, upon increasing the concentration of CS from 2 to 7%, we observe a highly viscous nanocomposite. Therefore, by considering the entrapment efficiency (EE) and loading capacity (LC) among F1, F2, F3, and F4, an optimized formulation was chosen for further characterization studies. From Table 1, F1 shows good EE for both LP and TM of 94.51% and 74.08%, respectively. In addition to this, F2 showed good EE for TM, and F3 exhibited the same for LP due to the variation in CS concentrations. In comparison, F4 shows the lowest EE and LC for both LP and TM. The decrease in the EE percentage of TM is expected due to the more hydrophilic nature of the drug. Furthermore, by considering EE and LC, the F1 composition was characterized and drug release was evaluated with different concentrations of Lyz.

3.1.1. Spectral studies. The optimized drug nanocomposite was analyzed by UV-visible spectroscopy—the appearance of a peak around 299 was observed for GQDs, whereas polyethyleneimine (PEI) and succinic acid (SA) peaks were found around 250 nm due to the absence of continuous conjugation as reported (Fig. 1A).[45,46] For CS, no significant absorption was reported; however, one shoulder peak at 254 nm and a broad peak (275 nm–483 nm) centered at 291 nm was found for amide linkages and the chromophoric C=O group. Furthermore, LP absorption was found at 210 nm, which could not be differentiated due to its weak absorption wavelength, and the TM peak was recorded at 295 nm. Therefore, we have observed that the broader peak can be attributed to the formation of the drug nanocomposite. In brief, we observed the broad peak from 271 nm to 348 nm centered at 294 nm and used the long chain, similar to CS, to confirm drug loading. Furthermore, through FT-IR and HPLC detection methods we have found the presence of the drugs. It is interesting to note
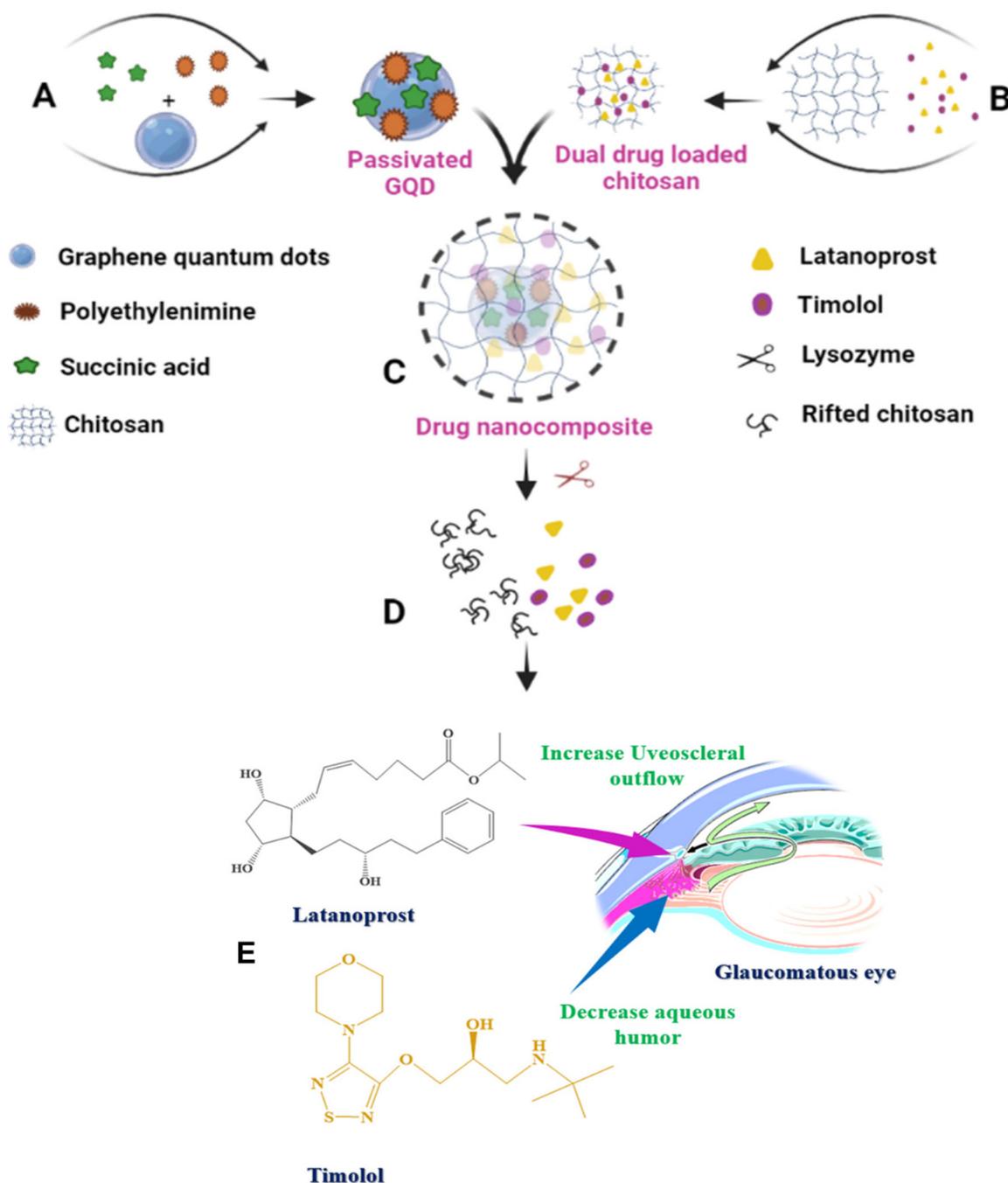
Scheme 1 Schematic representation of the development of drug nanocomposite and lysozyme responsive cleavage: (A) preparation of passivated GQD, (B) dual drug embedded chitosan, (C) drug nanocomposite, (D) lysozyme responsive cleavage, and (E) mechanism of action of latanoprost (LP) and timolol (TM) at the ocular region of the glaucomatous eye.

Table 1 Formulation of the drug (LP–TM) nanocomposites and their entrapment efficiencies and loading capacity percentages

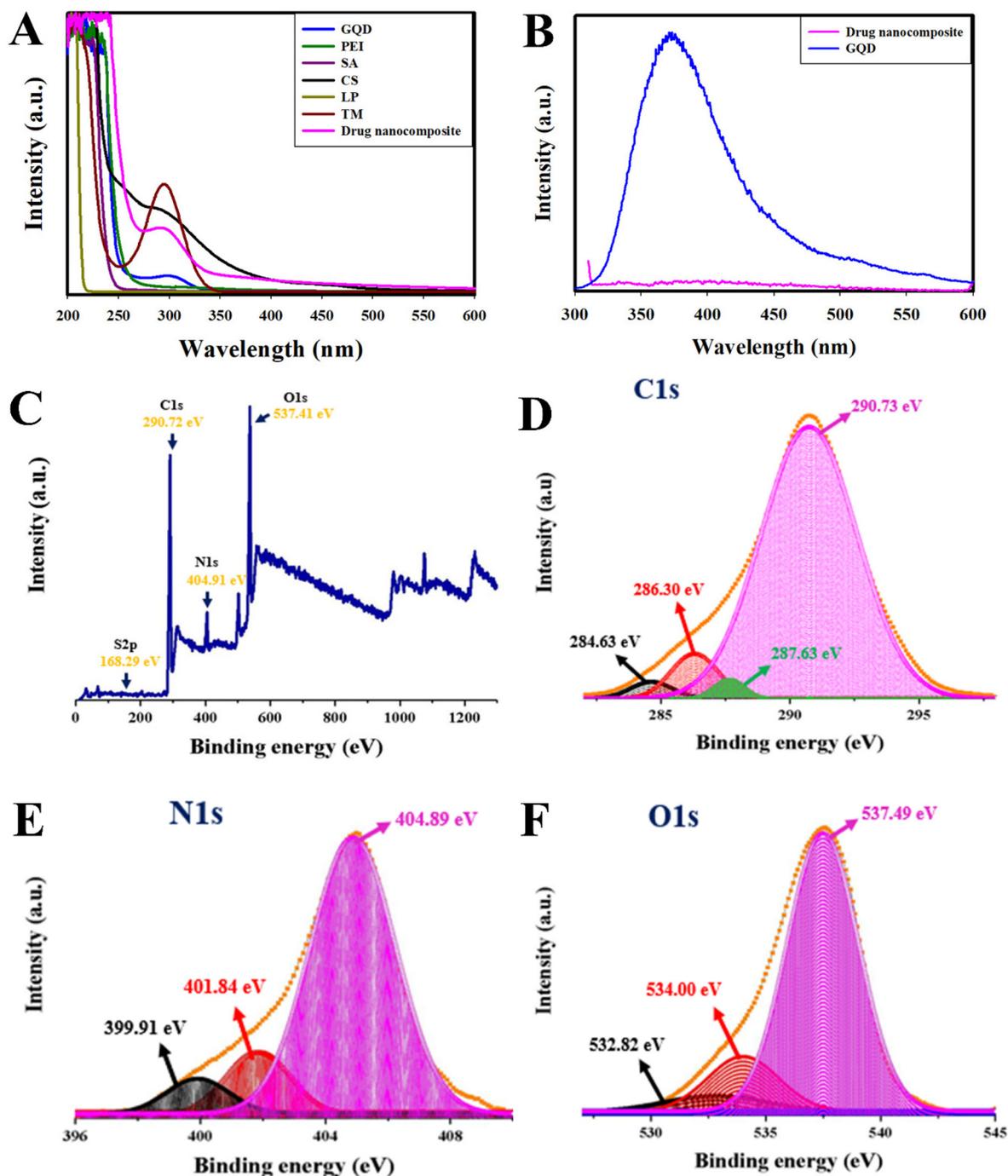| Sl. no	GQD (µL)	PEI (mg)	SA (µL)	Chitosan (%)	Amount of LP loaded (µg)	Amount of TM loaded (µg)	Entrapment efficiency (LP : TM, % EE)	Loading capacity (LP : TM, % LC)
F1	50	5.46	90	2	30	600	94.51 : 74.08	0.092 : 1.452
F2	50	5.46	90	3	30	600	89.06 : 74.29	0.088 : 1.456
F3	50	5.46	90	5	30	600	97.93 : 60.51	0.095 : 1.186
F4	50	5.46	90	7	30	600	86.38 : 56.75	0.084 : 1.112

Fig. 1 (A) UV-visible spectral data, (B) emission spectral data, (C) XPS survey scan spectrum of drug nanocomposite, (D–F) high-resolution deconvoluted spectra of C 1s, N 1s, and O 1s of the drug nanocomposite.

that, by considering the PL property, GQDs have been employed to track the drug loading and through spectral variations in fluorescence drug encapsulation could be confirmed. Practically, the single carbon precursor, graphene oxide (GO), oxidizes to form GQDs at 120 °C in the presence of strong acids, which exhibit blue fluorescence under UV light. Therefore, no intermediates form using the top-down preparation methods with GO. Hence, we have used the top-down method to synthesize the GQDs and utilized them for drug delivery applications. In the present study, emission spectroscopic studies were carried out to confirm the variation in fluorescence and drug loading in comparison with pristine GQDs. The quenching of the PL in the drug nanocomposite was observed due to the increased influence of polymer matrices, which were believed to have a stronger effect on surface electronic structures, resulting in changes to the energy gaps. In

addition to this, there is a redshift (~24 nm) in the PL peak centered at 401.77 nm for the drug nanocomposite, whereas the peak at 377.2 nm represents GQDs (Fig. 1B). Due to variations in the emission peak, the band gap has shifted from 3.28 eV (GQD) to 3.08 eV (drug nanocomposite), which is expected for a stronger effect on the surface electronic structures. Besides, we have also observed ~99% quenching of the PL in the present study compared to the previous report probably due to CS polymer encapsulation and the synergistic effect of dual drugs. To evaluate the decrease in fluorescence intensity upon drug loading, a fluorescence lifetime study was carried out for GQDs and the drug nanocomposite (Fig. S1†). Generally, the lifetime of a fluorescent species can be determined from the decay of its fluorescence intensity as a function of time. The average lifetime of the GQD was found to be 0.54 ns, and it exhibited 3 components: 2.30 ns (τ_1), 0.37 ns (τ_2), and 6.88 ns (τ_3) under excitation at 295 nm in solution. Similarly, the drug nanocomposite demonstrated an average lifetime of 0.22 ns, which showed 3 components: 1.92 ns (τ_1), 0.17 ns (τ_2), and 7.64 ns (τ_3) under the same conditions. Hence, the addition of drug loaded CS to the fluorescent nanomaterial shortened the lifetime and reduced the fluorescence intensity. The obtained data are in concordance with the fluorescence spectral and band gap studies.

3.1.2. XPS analysis. The variation in the atomic percentages in comparison with the LP-loaded nanocomposite proved the loading of TM into the nanocomposite. For the dual drug-loaded nanocomposite (drug nanocomposite), the XPS survey scan spectrum shows the presence of different elements in the nanocomposite (Fig. 1C). The peaks at 404.91 eV, 537.41 eV, 290.72 eV, and 168.29 eV are responsible for N 1s, O 1s, C 1s, and S 2p with atomic percentages of 7.19, 23.9, 68.83, and 0.07, respectively. Furthermore, the O/C value is found to be 0.34 for the drug nanocomposite. The deconvoluted C 1s spectrum demonstrates the presence of C=C, C–C, and C–O–C functional groups, whereas that of N 1s represents the formation of graphitic, pyrrolic, and amino nitrogen groups. Furthermore, the deconvoluted O 1s spectrum confirms the presence of C=O, C–O–C, and COOH functional groups. In brief, the deconvoluted high-resolution C 1s spectral peaks (Fig. 1D) at 284.63 eV are responsible for C–C/C=C, 286.30 eV is due to the presence of C=N, 287.63 eV is accountable for C=O/COOH and 290.73 eV is exclusively for O–O=C functional groups, respectively. The N 1s spectral peaks present at 399.91 eV are responsible for amino 'N', 401.84 eV for graphitic 'N', and 404.89 eV for nitro 'N' functional moieties (Fig. 1E). In addition to this, O 1s peaks (Fig. 1F) at 532.82 eV occurred due to C–O–C/C–O, 534.00 eV for C–OH, and 537.49 eV is responsible for adsorbed O_2/C as per the NIST database. Therefore, the functional groups present in different regions elucidate the dual drug loading and the deconvoluted S 2p peak usually appears at 165 eV (within the survey scan of S 2p at 168.29 eV) represents the presence of the N–S–N functional group due to the loading of TM.

3.1.3. FT-IR analysis. FT-IR spectral studies were performed to analyze the presence of TM and LP in the drug

nanocomposite. For the TM drug, N–H stretching and –OH stretching vibrations appeared in the regions of 3366 cm^{-1} and 3246 cm^{-1}, respectively. The CH bending vibration was observed at 1386 cm^{-1}; the peak at 1626 cm^{-1} corresponds to the C=O stretching vibration, and those at 1540 cm^{-1} and 1459 cm^{-1} are responsible for C=C aromatic rings as reported.[31,47] In brief, the drug nanocomposite exhibited broadened peaks at 3339 cm^{-1} to 3259 cm^{-1} for –NH and –OH functional groups. The occurrence of LP in the composite was further confirmed with the distinct broad peak for aliphatic C–H stretching centered at 2880 cm^{-1} and ester C–O stretching vibrations at 1299 cm^{-1}. The peaks associated with C–N stretching of the amide bond, asymmetric C–O–C, and C–O stretching vibrations are observed at 1366 cm^{-1}, 1159 cm^{-1}, and 1073 cm^{-1}, respectively. Interestingly, we have also spotted that the sharp peak at 1626 cm^{-1} represents the presence of the amide C=O bond stretching peak responsible for the occurrence of CS (Fig. S2†). Therefore, the above-mentioned spectral vibrations are in complete accordance with the presence of LP and TM in the drug nanocomposite.

3.1.4. Particle size and mucoadhesiveness analysis. The dynamic light scattering (DLS) technique was used to study the particle size of the prepared drug nanocomposite. The particle size of the pristine GQD was found to be 1.7 nm[32] whereas the size of the drug nanocomposite (Fig. 2A) was 490 nm. It should be noted that ≤500 nm particle-sized drug-loaded composites are highly suitable for ocular delivery applications.[48]

To evaluate the mucoadhesive nature, we mixed an equal volume of mucin nanoparticles and drug nanocomposite, resulting in the formation of an aggregated structure with a particle size of 1584 nm, whereas it was 291 nm for mucin. The massive increase in particle size proves the interaction of the drug nanocomposite with mucin particles. The obtained results prove that nanocomposites can reside for longer in the cornea by binding with sialic acid present in the mucosal layer, which results in the prolonged delivery of drugs to decrease IOP thereby managing glaucoma.

3.1.5. Surface morphological (HR-TEM and FE-SEM) studies. A high-resolution transmission electron microscopy (HR-TEM) study was performed to evaluate the surface morphology of the nanocomposites. Herein, CS appears as a plain sheet (Fig. 2B). The addition of dual drug-loaded CS to passivated GQDs results in the formation of an aggregated structure with an enhanced size (Fig. 2C). As a result of more aggregated structures, we found an increase in the particle size for the drug nanocomposite. The obtained results from the HR-TEM analysis agree with the obtained DLS data, wherein an increment in the size of the drug nanocomposite is observed. Furthermore, a selected area electron diffraction (SAED) study confirms the polycrystalline nature of the nanocomposite (Fig. 2D).

Furthermore, we performed FE-SEM analysis (Fig. S3†) to identify the surface morphology of the drug nanocomposite. From the data, we could identify the presence of drugs in aggregated form; this is similar to the results obtained from the HR-TEM studies. In addition, energy-dispersive X-ray spec-
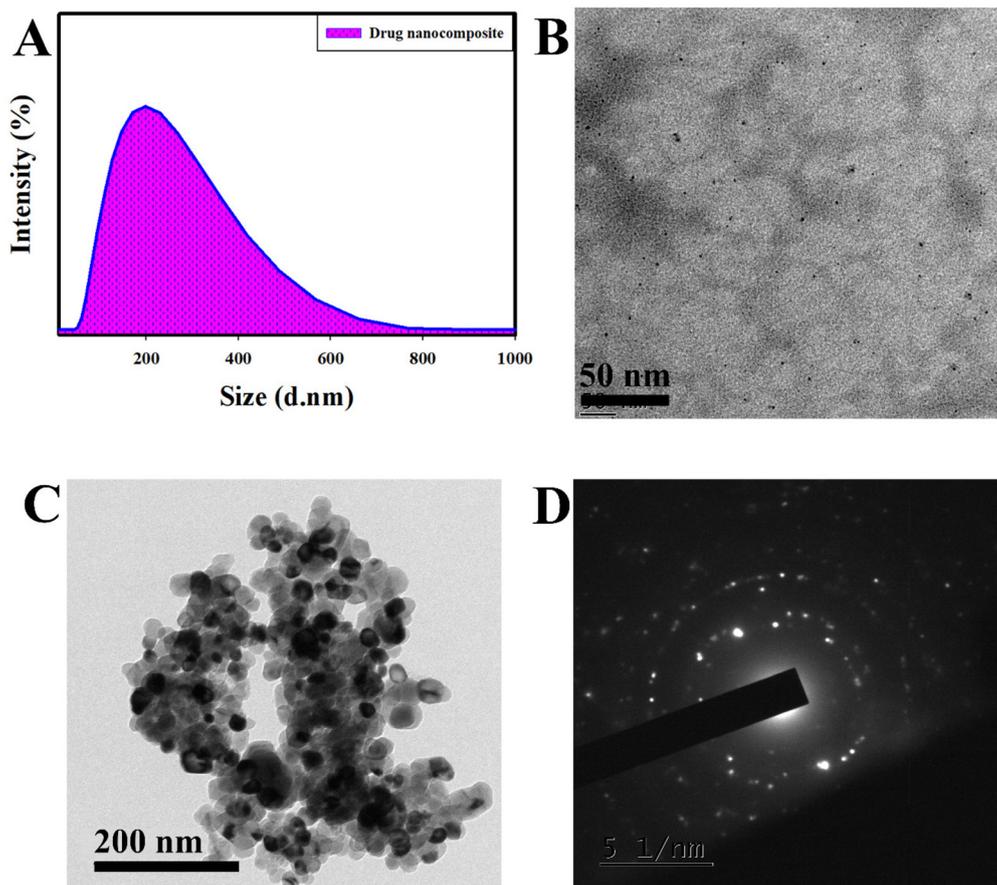
Fig. 2 (A) Particle size analysis of the drug nanocomposite, (B and C) HR-TEM image of chitosan at 50 nm magnification and drug nanocomposite at 200 nm magnification, and (D) selected area electron diffraction (SAED) pattern of the drug nanocomposite.

troscopy (EDS) and elemental mapping studies for GQD, LP, TM, and drug nanocomposites were carried out (Fig. S4 and S5†). It was observed that GQD showed the presence of C, N, O, and S due to the utilization of graphene oxide as a precursor in the presence of HNO_3 and H_2SO_4.[32] Furthermore, C and O were observed for the LP drug (molecular formula (MF): $C_{26}H_{40}O_5$) with 33.33 at% C and 66.67 at% N, whereas C, O, N, and S were found for TM (MF: $C_{13}H_{24}N_4O_3S$; 27.71 at% C, 55.43 at% O, 10.65 at% N, & 6.20 at% S). For the drug nanocomposite, we found the presence of C, N, O, and S due to the presence of the synthesized material and drugs. The observed elemental compositions of GQD and drug nanocomposites agree with the XPS analysis in section 3.1.2.

3.2. *In vitro* drug loading and release studies

Drug release studies were conducted to evaluate the Lyz-responsive simultaneous release of LP and TM. LP and TM have different mechanisms of action in dealing with IOP, as shown in Scheme 1E.

The drug release studies were quantified using HPLC at two different wavelengths simultaneously. It was found that at 300 μg mL^{-1} Lyz treated nanocomposite delivered 23.10% and 35.71% of the drug in 72 h with burst releases of 1.04% and

4.72% in 1 h for LP and TM. Whereas in the case of 600 μg mL^{-1} Lyz treated nanocomposite, the delivery was found to be 29.54% and 42.86% of the drug in 72 h with 5.72% and 13.87% burst releases in the first hour respectively. Importantly, 1000 μg mL^{-1} Lyz-treated nanocomposite exhibited burst releases of LP and TM of 11.77% and 17.32% in an hour and sustained release of 32.68% and 66.61% of the drugs in 72 h, respectively (Fig. 3A and B). Furthermore, to understand the drug release response, a comparison study of the drug nanocomposite and individual commercial formulations was carried out by taking similar concentrations. The commercially available latoprost eye drops released around 84% of the drug within 1 h and complete drug release was observed within 2 h. Similarly, 89.44% of TM was released from the Timolet eye drops in 12 h, and the remaining drug was released within 24 h of the study (Fig. 3C) Therefore, in comparison with commercial formulations, the drug nanocomposite could act efficiently at managing glaucoma.

The drug release kinetics was analyzed by overlapping the obtained data with various kinetic models. Furthermore, the possible release kinetics was determined by considering the high coefficient of regression (R^2) as shown in Table 2; related equations are given in the ESI.†
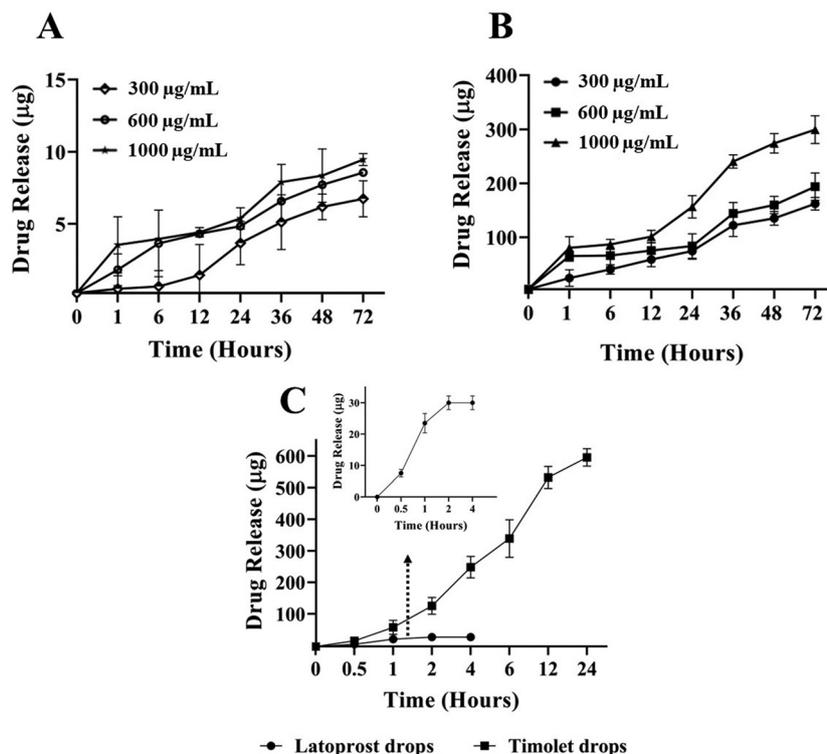
Fig. 3 *In vitro* simultaneous release of (A) LP and (B) TM from the drug nanocomposite in the presence of lysozyme, and (C) drug release study of commercially available latoprost and Timolet eye drops.

Table 2 *In vitro* drug release kinetics of dual drug-loaded nanocomposites

Model	Parameter	LP			TM		
		300 μg mL⁻¹ Lyz	600	1000	300 μg mL⁻¹ Lyz	600	1000
Zero order	R^2	0.9172	0.9235	0.9427	0.7943	0.8207	0.4999
First order	R^2	0.7636	0.7663	0.9146	0.6989	0.8121	0.4923
Hixson–Crowell	R^2	0.8300	0.8313	0.9256	0.7388	0.8156	0.4948
Korsmeyer–Peppas	R^2	0.9305	0.9818	0.8292	0.8073	0.8246	0.8689
	n	0.8499	0.3777	0.2537	0.4021	0.1352	0.0691

The obtained results from the models show that the release kinetics follow zero order and Korsmeyer–Peppas models for both released drugs; this demonstrates that drug release is independent of the concentration of the drug present. Interestingly, at a lower concentration of Lyz (300 μg mL⁻¹), LP drug release was observed to follow a non-Fickian or anomalous transport mechanism due to the involvement of more than one mechanism (release exponent, $n > 0.45$), whereas the remaining drug release was observed to follow the Fickian diffusion mechanism (release exponent, $n < 0.45$). The Fickian mode of diffusion was significant for TM, possibly due to the hydrophilicity of the water-soluble drug during dual drug release. The obtained kinetics results are in accordance with the proposed mechanism in our study that Lyz is involved in the release of the drug by cleaving the β-1,4 glycosidic linkages of CS, possible diffusion of the drug, and transport of the drug

through the concentration gradient due to the swelling nature.[31,32] The Hixson–Crowell model reveals that the reduction in the surface area or the decrease in the diameter of the nanocomposite during release, which can be observed in our study because drug release occurs upon cleavage of the nanocomposite, results in the formation of fragmented CS.[49]

Furthermore, a field emission-scanning electron microscopic (FE-SEM) study was conducted to observe surface morphological changes due to the Lyz accelerated degradation/cleavage of the nanocomposite. The Lyz action varies with respect to pH (active at pH 6.0–9.0) and concentration. Herein, we studied the degradation of a nanocomposite at pH 7.4 with a higher concentration of Lyz (1 mg mL⁻¹) for 24 h of incubation. In the absence of Lyz (Fig. 4A and B), we could observe a clear and flat surface with connected networks of polysaccharide layers. Upon treatment with Lyz, the degradation of
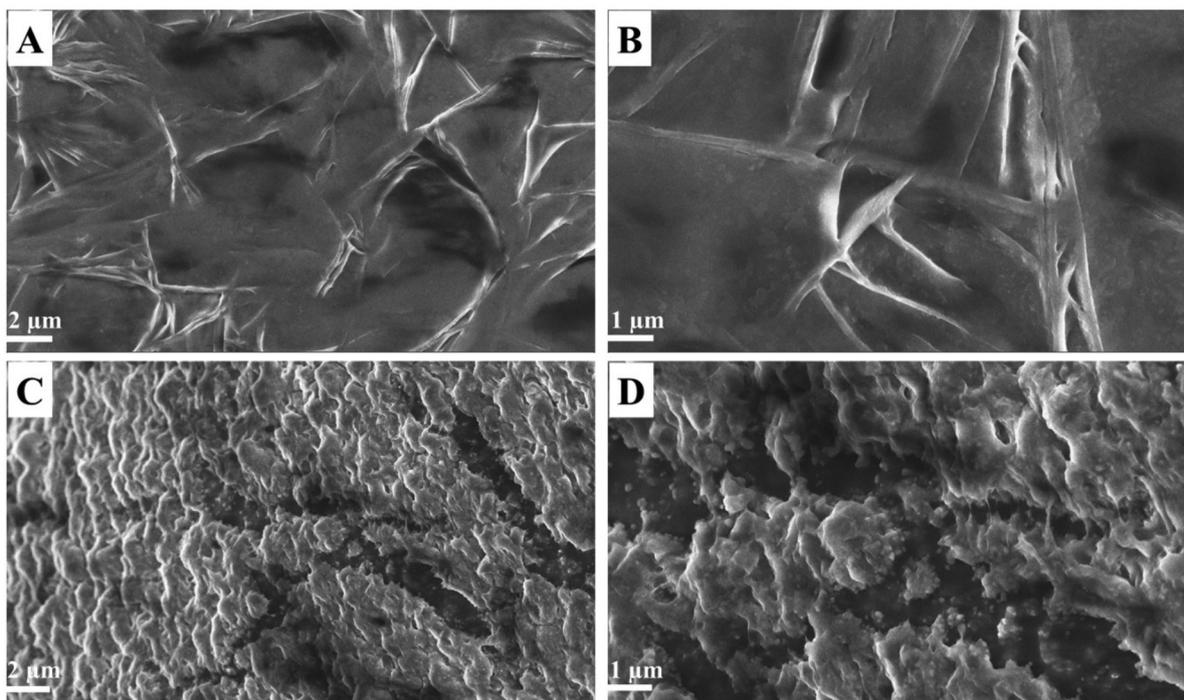
Fig. 4 (A and B) FE-SEM images of the drug nanocomposite (2 μm and 1 μm magnification) and (C and D) lysozyme treated drug nanocomposite (2 μm and 1 μm magnification).

the nanocomposite can be seen by the formation of the cracked and uneven surface (2 μm and 1 μm magnification) in Fig. 4C and D, which leads to the release of dual drugs. Several studies reported the utilization of CS and its hydrogels, scaffolds, and *in situ* gel as a platform to deliver drugs for various skin, cartilage, and bone tissue engineering applications.[50,51]

In addition, we characterized the released fragmented CS upon Lyz treatment by ^{1}H-NMR spectral studies, as discussed in the following section, and identified the cleavage site and the formation of hydroxyl groups spectroscopically.

3.3. Characterization of the products released from the nanocomposite upon treatment with lysozyme

The ^{1}H-NMR spectral study was performed to evaluate the chemical structure of the material released from the drug nanocomposite in the presence and absence of Lyz as shown in Scheme S1.† The prepared composites were dissolved in D_2O, in which the peak appears in the region of 4.7 ppm. For the Lyz-treated drug nanocomposite, the CS peaks positioned at 2.2–2.6 ppm are determined to be multiplets of CH_2 and at 3.0 ppm for the triplet of CH. The peaks at 3.1–3.8 ppm are associated with CH_2OH and CHOH, and the peak at 1.2 ppm is responsible for the terminal triplet of CH_3. It is noteworthy to mention that the peaks present for the drug nanocomposite (Fig. 5A), Lyz-treated drug nanocomposite (retentate) (Fig. 5B), and degraded (dialyzed) (Fig. 5C) nanocomposites were found to be almost the same except for some peak shifts; similar kinds of chemical shifts were observed previously for lysozyme

based insulin drug delivery in chitosan systems.[52] However, we observed a new peak at 3.8 ppm in the degraded nanocomposite (Fig. 5C), which was attributed to CHOH due to the hydrolysis of the β-1,4 glycosidic bond, followed by the formation of fragmented low molecular weight CS. In the Lyz-treated drug nanocomposite, we were unable to find a similar peak formation, probably due to the formation of the enzyme–substrate complex or interactions. The above-mentioned ^{1}H-NMR data confirm that the drug nanocomposite in the presence and absence of Lyz is almost the same, which proves the formation of CS nanomicelles or fragmented CS without the formation of by-products.

3.4. *In vitro* cytocompatibility, bright field imaging, and live/dead cell staining assay

To assess the toxicity of the prepared composites, we performed an *in vitro* cytocompatibility (MTT) and live/dead (AO/EB) staining assay against human corneal epithelial (HCE) cells. The phenotype of the *in vitro* primary HCE cells has a better match with the *in vivo* tissues. Furthermore, these cultures of corneal cells will predict toxic reactions in the intact cornea *in vivo*.[53] Therefore, the toxicity of the nanocomposite can be obtained by using cultured HCE cells. The *in vitro* MTT assay data in Fig. 6A and B demonstrate that the prepared composites (drug nanocomposite and Lyz-treated drug nanocomposite) are found to be viable towards HCE cells by providing more than 80% viability for concentrations from 20 to 100 μg mL^{-1}.
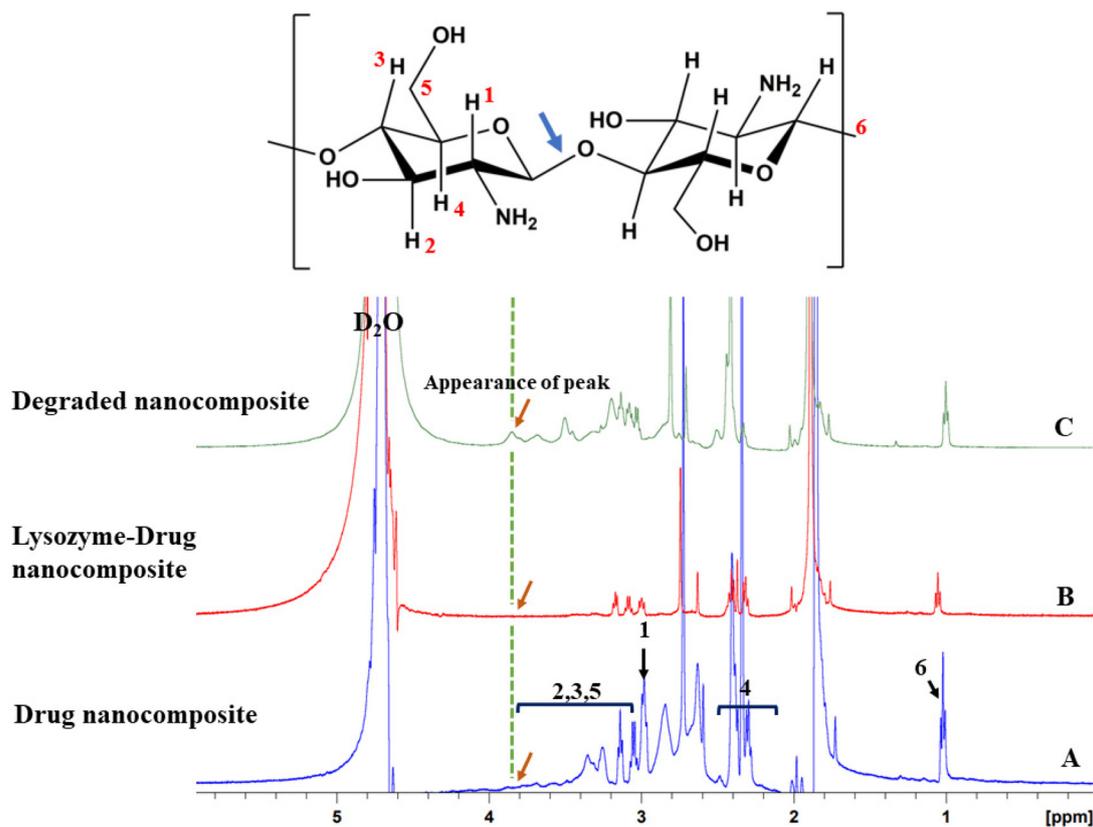
Fig. 5 ^{1}H-NMR spectral peaks of (A) drug nanocomposite, (B) Lyz-treated drug nanocomposite (retentate), and (C) degraded nanocomposite (after dialysis).

To check for morphological changes, different concentrations of nanocomposites (drug nanocomposite and Lyz-treated drug nanocomposite) such as 20, 60, and 100 μg mL^{-1} were tested against HCE cell lines (Fig. 6C and S6†). The results show that there are no significant changes to the morphology of the cells and they are found to be structurally intact upon incubation for 24 h at all treated concentrations due to the biocompatible nature of the composite. Furthermore, cells were counted and the results are displayed in Fig. S6.†

Furthermore, to check the stages of apoptosis, we performed an AO/EB staining assay with similar concentrations of 20, 60, and 100 μg mL^{-1} of nanocomposite (drug nanocomposite and Lyz-treated drug nanocomposite), in which the prepared composite did not show any apoptosis stages of the cells (Fig. 7 and S7†). Additionally, we did not observe the cells in the red field, and the absence of yellow or red fluorescent cells in the merge field followed by the appearance of green-stained cells exclusively determines the viable nature of the cells. Moreover, all the treated nanocomposites are found to be biocompatible in all the *in vitro* biological studies.

3.5. HET-CAM assay

All the *in vitro* cytotoxicity evaluations confirm that the composites are biocompatible and the cells are viable. Furthermore, to use the formulation for ocular applications, a Draize test

must be conducted to evaluate ocular irritation, therefore, as an alternative to the *in vivo* Draize rabbit eye test, herein, we have used the hen's egg analysis using the chorioallantoic membrane (HET-CAM test). The CAM of the chick embryo has several tissues including arteries, capillaries, and veins, which help to provide similar results to conjunctival tissue on inflammation. As a preliminary observation, we performed a HET-CAM assay to evaluate the ocular irritation of the prepared materials and nanocomposites.[40] To evaluate ocular irritation, we have taken GQD, passivated GQD, CS, LP, TM, and LP-loaded drug nanocomposite and the drug nanocomposite. It was observed that none of the tested materials except the positive control (NaOH) showed any haemorrhage (HM), clotting (CL), or hyperemia (HY) in the CAM upon exposure for 5 min with an irritation score (IS) of 0; hence, they can be considered safe for ophthalmic use (Fig. 8). As mentioned, treatment with 0.1 M NaOH caused severe irritation (IS of 11.06) from 0 min to 5 min.

3.5.1. Histopathological studies. The histopathological examinations of the CAM in Fig. 9 showed the presence of healthy blood vessels (HBV), primary capillaries (PC), secondary capillaries (SC), and tertiary capillaries (TC) in all the tested individual compounds and formulations. However, shrunken blood vessels (SBV) and reduced capillaries (RC) were found in the positive control treated CAM due to severe
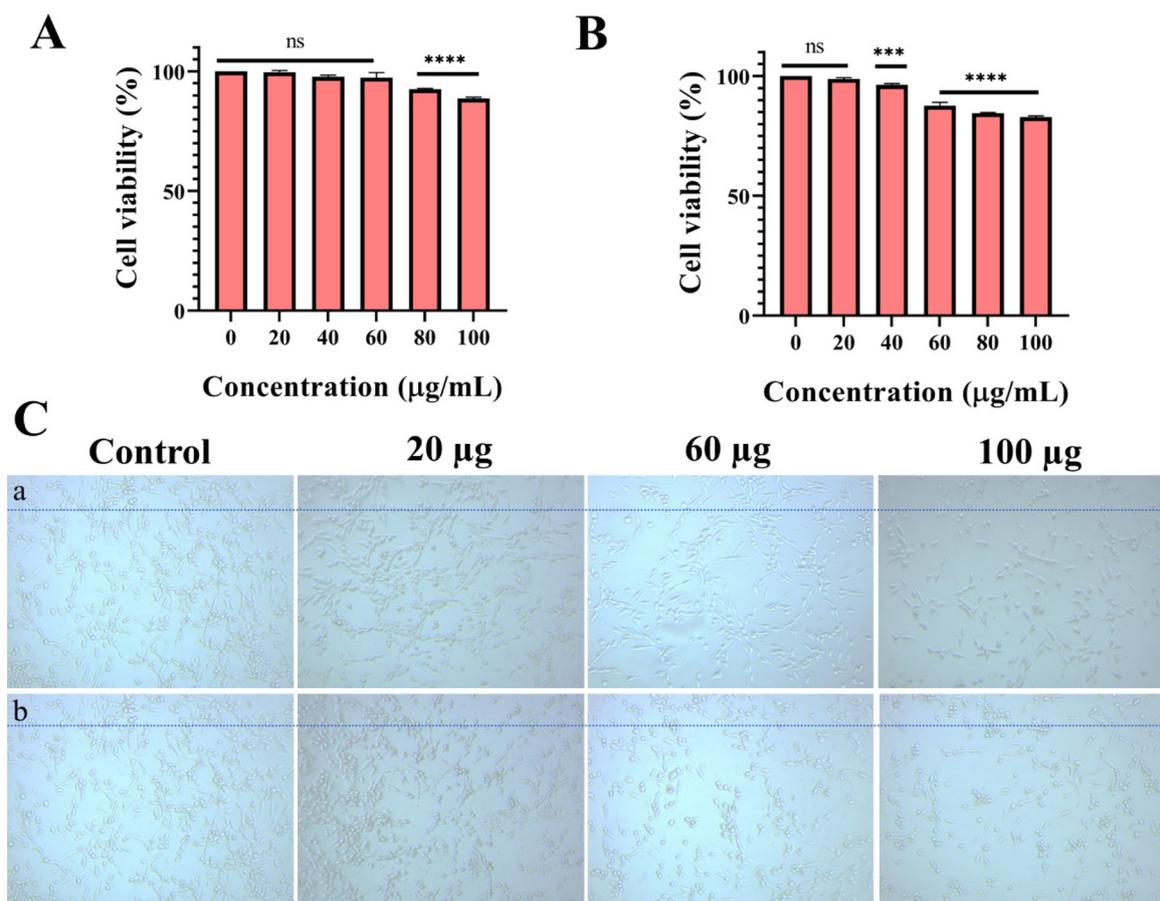
Fig. 6 *In vitro* biocompatibility assay of (A) drug nanocomposite, and (B) Lyz-treated drug nanocomposite with concentrations of 20–100 µg mL^{-1} (statistical significance was assumed for *p*-values: ns = non-significant, *P < 0.05, **P < 0.01, ****P < 0.0001; Statistical significance were plotted in comparison to control), and (C) bright field image of (a) drug nanocomposite, and (b) Lyz-treated drug nanocomposite at 20, 60, and 100 µg mL^{-1} against HCE cells (20× image magnification).

irritancy that led to damaged blood vessels. The treated compounds, namely, GQD, passivated GQD, CS, LP, TM, LP-loaded nanocomposite, and the drug nanocomposite showed the presence of normal growth of blood vessels without any differences. Hence, the histopathological study confirms the non-irritancy of the prepared composites. Furthermore, we counted the number of PC, SC, and TC to observe differences in comparison with the positive control. We found that the positive control had SBV and a limited number of PC, SC, and TC. Therefore, the graph provided in the ESI† (Fig. 10) proves that all the precursors and drug nanocomposites except the positive control have a good number of capillaries, which proves non-irritancy.

3.6. Molecular docking

Molecular docking studies (Fig. 11) were performed to visualize the interactions and binding affinity of the drugs (LP and TM) with CS by using AutoDock Vina 1.5.6. The polymer, CS, has reactive amine groups; hence it facilitates inter- and intramolecular interactions towards neighbouring molecules.[54] For the interactions of CS and LP, we observed 1 hydrogen bond

(non-classical) with the lowest binding energy of −6.0 kcal mol^{-1} having the 6 best interactions. The length of the H-bond was found to be 2.74 Å. Non-classical bonds are usually found in carbohydrates connected by π-electrons and we have elucidated that CS encapsulates the LP through π–π stacking interactions. Furthermore, the CS and TM exhibited the lowest binding energy of −5.9 kcal mol^{-1} and are connected by 5 hydrogen bonds and electrostatic interactions, and showed 9 modes of interactions. For this, the H-bond lengths were found to be 3.04, 2.96, 2.89, 3.07, and 3.16 Å. It is very evident that due to its hydrophobic nature, LP showed fewer interactions with CS; however, TM was found to exhibit more hydrogen bonds due to the presence of hydrophilic moieties, as seen by the resulting low binding energy for TM (−5.9 kcal mol^{-1}). Generally, a low binding score depicts effective interactions of the drug with the polymer. In the case of LP and TM interactions, we noted 9 binding modes with the lowest binding energy of −3.4 kcal mol^{-1}. For this, we observed 1 hydrogen bond with a length of 1.40 Å and 2 electrostatic interactions. The probable electrostatic interactions provide the repulsion against attractive forces to prevent aggregation.[54]
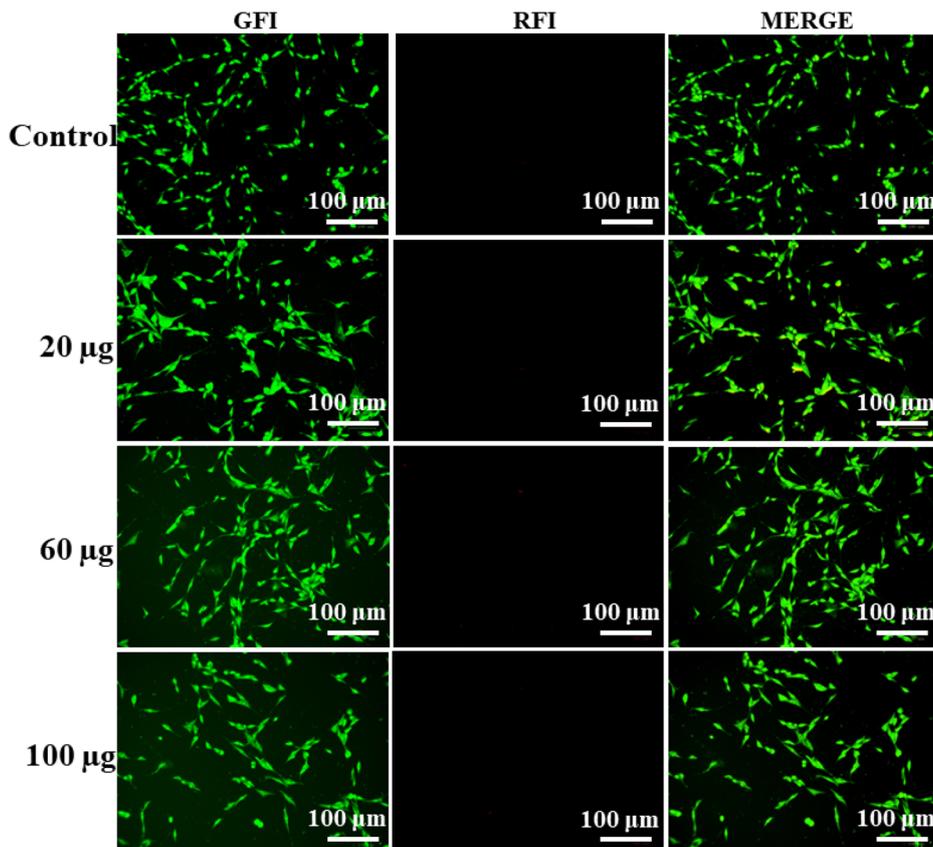
Fig. 7 *In vitro* AO/EB staining images of drug nanocomposite against HCE cell lines with concentrations of 20, 60, and 100 µg mL^{-1}. Images were captured after 24 h of drug treatment (image magnification = 100 µm).

Hence, a detailed molecular docking study showed the interactions of LP and TM towards the polymer chain and the formation of a stable structure.

4. Discussion

The optimized dual drug-loaded nanocomposite was considered for optical and surface morphological characterization studies. Several publications described the utilization of fluorescent carbon dots and GQDs for anti-cancer drug delivery applications.[55,56] In brief, Srivastava *et al.*[57] and Misra *et al.*[58] reported the use of caged PL carbon nanoparticles for sensing and drug delivery in response to UV light and counter ionic ligands by reverse switching of the PL. Interestingly, in our previous work, we demonstrated the reverse switching phenomenon in the presence of an ocular enzyme, Lyz, by taking LP as a model drug.[32]

In the present work, GQDs were employed to develop the nanocomposite, and by considering the PL property of the same, drug loading was confirmed by PL spectral studies. Quenching of the PL central peak at 401.77 nm suggests LP and TM loading into the nanocomposite and the redshift supports for the same. Similar results were seen in our previous

work with the ~18 nm redshift in the peak.[32] The broader variation in the redshift from ~18 to ~24 nm also points to the dual drugs being present in the nanocomposite. The PL spectral variations change the band gap due to variations in the surface electronic structures. The PL decay study also confirms the decrease in the decay time from 0.54 ns to 0.22 ns, suggesting that quenching of the fluorophores is responsible for emission. It should be noted that similar PL lifetime changes are observed for quantum dots bio-conjugated with proteins for drug release in the presence of maltose[59] and fluorescence quenching with respect to bio-conjugated carbon quantum dots.[60] Moreover, the decrease in average lifetime is a consequence of caged GQDs inside the chitosan–drug nanocomposite. It has been reported that the microenvironment surrounding the GQDs also results in a reduction of the mean lifetime.[61] Hence, the addition of drug loaded CS to the fluorescent nanomaterial shortened the lifetime and decreased the fluorescence intensity. The obtained data are in concordance with the fluorescence spectral and band gap studies.

XPS analysis confirms the variations in the binding energy concerning new bond formations and alterations of the functional groups upon modification. The XPS analysis of GQD and passivated GQD showed the presence of C, N, O, and S.[32] For the LP-loaded nanocomposite, we observed C 1s, N 1s, and
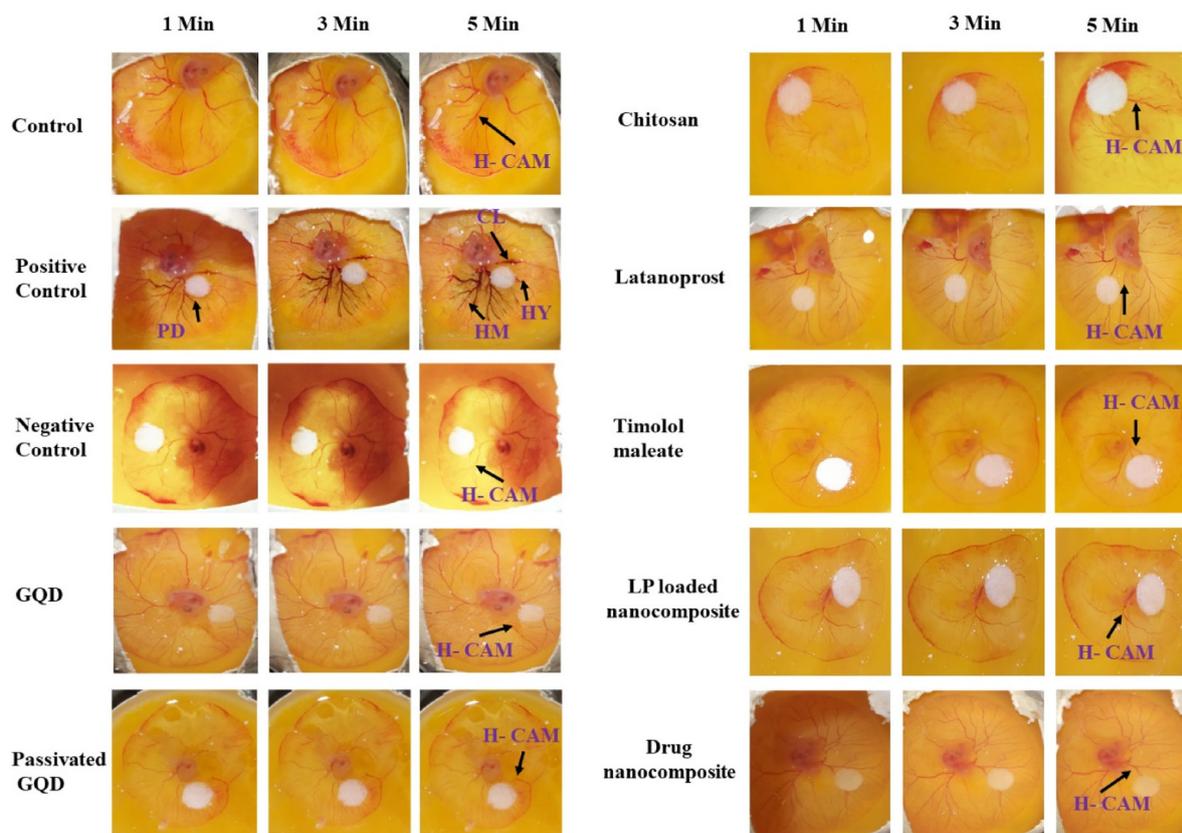
Fig. 8 Hen's egg chorioallantoic membrane treated precursors and formulations: control, positive control (0.1 M NaOH), negative control (0.9% NaCl), GQD, passivated GQD, CS (2%), LP, TM, LP loaded nanocomposite, and the drug nanocomposite under observation for 5 min (H-CAM: healthy CAM, PD: paper disk, HM: haemorrhage, HY: hyperemia, CL: clotting).

O 1s at binding energies of 284 eV, 401 eV, and 532 eV with atomic surface percentages of 56.18, 2.39, and 28.37, respectively. Similarly, the LP–TM-loaded nanocomposite demonstrated the presence of C, N, O, and S. The difference in functional group formation compared to the LP-loaded nanocomposite represents the loading of dual drugs.

The formation of the nanocomposite and occurrence of the drugs could be found through X-ray diffraction (XRD) analysis as an alternative to the above-mentioned methods. In brief, XRD is a basic analytical technique used to identify and characterize the phase from its diffraction pattern. As mentioned in a few reports in the literature, GQDs obtained from GO demonstrate a highly intense peak at 33.34° responsible for the high crystallinity of the material.[31] In addition to this, a few peaks could be found at 20.33°, 29.26°, 30.21°, 35.12°, and 39.76°.[62] The peaks responsible for pure CS could be observed from 10 to 30° with the peak centered at 20.94° with a shoulder peak at 16.22° being responsible for pure CS with planes of (220) and (110).[63] As reported, the presence of intermolecular and intramolecular hydrogen bonding is responsible for the rigid structure of CS.[64] Furthermore, TM shows intense peaks in various regions from 10 to 30° and especially high intensity at 20.17° responsible for the crystallinity of the drug.[33,65]

In the case of FT-IR spectra, the peaks responsible for the starting materials CS, LP, GQDs, and passivated GQDs were described in an earlier publication.[32] In the present study, similar peaks were found with a slight shift in the peak positions as a result of the successful drug loading of TM and LP in the composite.

In the case of particle size, maintaining a suitable size (≤500 nm) of the nanocomposite is necessary to prevent ocular irritation. It also increases the ocular bioavailability of the drug, as well as stabilizing the colloidal dispersion. It is interesting to note that the smaller particle size of the nanocomposite offers a greater surface area, which is an important criterion for the binding of nanoparticles or nanocomposite to the ocular surface.[66] The obtained particle size of the drug nanocomposite in the current study is 490 nm, which is necessary for ocular applications as per earlier reports. Very recently, Rubenicia *et al.* prepared LP eye drops loaded with hyaluronic acid–CS nanocomposite to treat glaucoma, wherein the particle size of the composite was found to be 314 ± 0.63 nm.[67]

CS is a polycationic, mucoadhesive material having a positive surface potential, and offers enhanced bioavailability of the drug by binding to the negatively charged mucus of the cornea.[31] The mucoadhesive contact is reinforced by
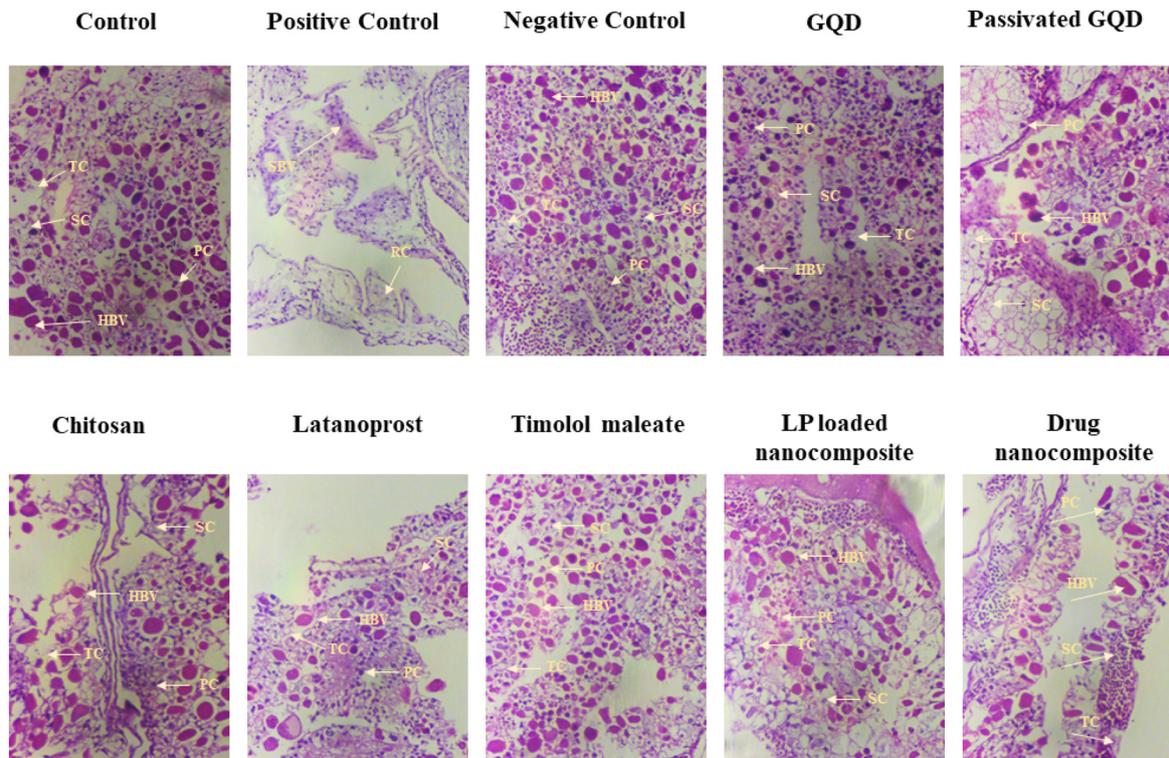
Fig. 9 Histological sections of chorioallantoic membranes (CAMs) treated with precursors and formulations under H & E staining. Images were captured under 20× magnification (HBV, healthy blood vessels; PC, primary capillaries; SC, secondary capillaries; TC, tertiary capillaries; SBV, shrunken blood vessels; RC, reduced capillaries).
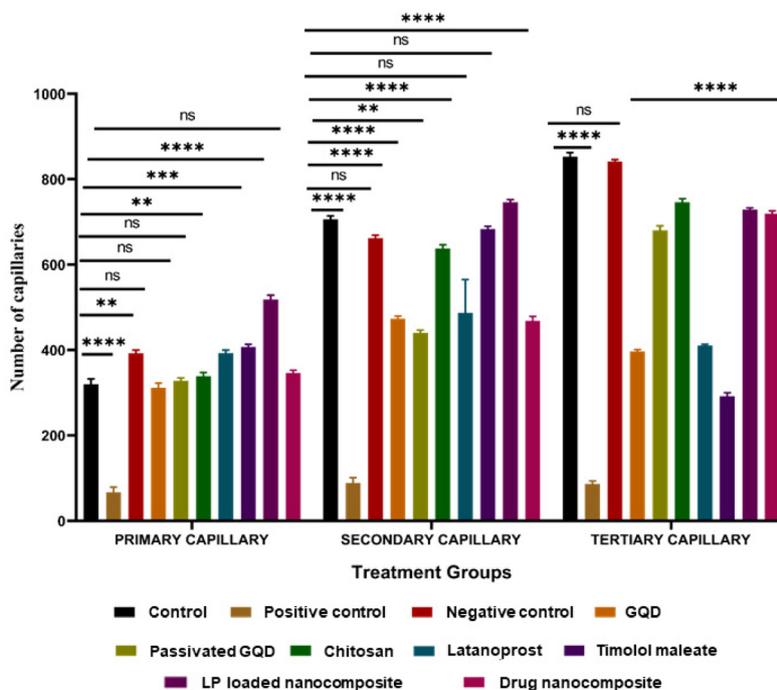

Fig. 10 Counts of primary capillaries (PC), secondary capillaries (SC), and tertiary capillaries (TC) of the treatment groups of HET-CAM analysis (statistical analysis: ns = non-significant, **$p < 0.01$, ***$p < 0.001$, ****$p < 0.0001$, mean $\pm$ SD, $n = 3$).
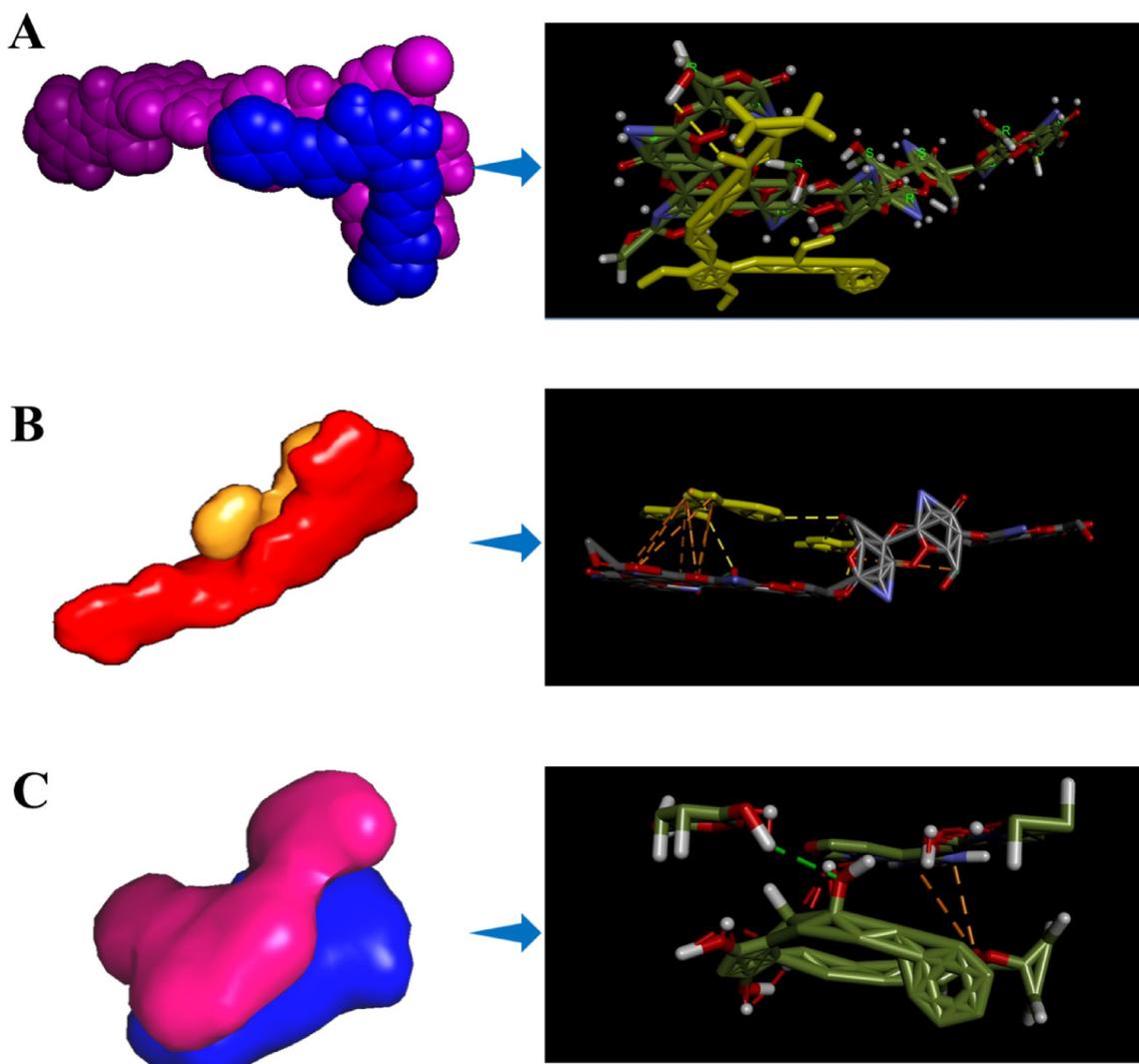
Fig. 11 Molecular docking model and bonding interaction representations of (A) chitosan–latanoprost, (B) chitosan–timolol, and (C) latanoprost–timolol.

interfusion across the formed interface when the drug nano-composite interacts with the mucus glycoprotein. The advantage of using cationic material is the mucoadhesive property of CS, and its effect on the protein-associated tight junctions leads to the prolonged ocular residence time and increased absorption of the drug.[32,68]

Mucoadhesive polymers are necessary to enhance corneal retention for a longer time and therefore, CS was employed in the current study. In brief, the pH and carboxylate groups present on the sialic acid of mucin play a critical role in the interaction with CS and its nanoparticles by protonation of the amino group to form electrostatic interactions and hydrogen bonds.

In the present study, an increment in the particle size to 1584 nm from 490 nm suggests the mucoadhesiveness of the developed drug nanocomposite. Similar results were reported by Pires de Sá *et al.*, wherein an increase in the particle size

from 96.5 ± 2.2 nm to 2441.3 ± 164.5 nm was observed after incubation with mucin due to the interaction between mucin and cationic-charged liposomal formulation.[35] Therefore, mucin interaction studies confirm that the drug nano-composite is mucoadhesive.

In the FE-SEM analysis, aggregated structures were found for the drug nanocomposite, while a planar sheet kind of surface morphology was determined for CS. The SAED pattern suggests the polycrystalline nature of the drug nanocomposite, which helps prolong drug delivery due to the disordered structure. The obtained surface morphological data agree with the XPS, DLS, and FT-IR studies. In addition, EDS analysis demonstrates the occurance of elements responsible for the drugs and drug nanocomposite similar to XPS analysis.

By considering the efficacy of dual drugs in treating glaucoma, simultaneous drug delivery analysis was carried out. Importantly, the simultaneous delivery of drugs will improve

patient compliance and reduce frequent administrations. The TM drug is administered twice a day with a commercial formulation concentration of 0.125%. Similarly, commercially available LP is usually administered once a day with a formulation concentration of 0.005% having an expected release of 1.5 μg day^{−1}. Xu *et al.* reported the co-delivery of LP and TM encapsulated polymeric micelles and found the burst release of 57.12 μg of TM and 0.70 μg of LP, and found no drug after 24 h. However, the dual drug-loaded micelles encapsulated in a contact lens showed an extended release time and promising decrease in IOP.[8] Wang *et al.* reported a co-drug deliverable multi-layered nanosheet by employing the spin coating method. In this, different drug release (25, 82, and 95%) performances were observed within 48 h for layered films in the presence of saline. From the commercial aspect, the application of nanosheets to the patient may require assistance.[15] In terms of mechanism, Lyz permeates into the drug nanocomposite layer-by-layer by cleaving the β-1,4 glycosidic bonds of chitosan, leading to the sustained delivery of the loaded drugs. Hence, we conceptualized the mucoadhesive stimuli-responsive release system, which could stand out as a trendy ocular nanocomposite and release the drugs simultaneously in the presence of naturally secreting enzymes sustainably for a longer time.

In the presence of lower and higher concentrations of Lyz, drug release was observed until 72 h. Maximum release was observed in the case of 1 mg mL^{−1} of Lyz and all the drug release patterns were dependent on the concentration of the enzyme. In addition, burst release in the first hour was found, possibly due to swelling and hydrolysis. In brief, Lyz activates the hydrolysis of β-1,4 glycosidic linkages[69] by recognizing the *N*-acetyl glucosamine sequences in the chitin/CS molecules; followed by increasing digestibility with the increasing degree of *N*-acetylation in the polymer chain.[70] At present, <5% of the applied formulations reach the cornea due to rapid lachrymation, hence the proposed system could show good pharmaceutical efficacy by releasing LP and TM simultaneously. It is noteworthy to mention that people who are suffering from dry eye syndrome will have a Lyz production of 0.7 ± 0.5 mg mL^{−1}, and healthy people have a mean tear Lyz production rate of 1.5 ± 0.5 mg mL^{−1};[71] therefore, we considered evaluating drug release of the nanocomposite by taking various amounts of Lyz (300–1000 μg mL^{−1}). In addition, *in vitro* release kinetics models suggest that the release is happening through the cleavage of β-1,4 glycosidic linkages of CS, possible diffusion of the drug, and transport of the drug through a concentration gradient due to the swelling nature.[31,32] The reduction in the surface area or the decrease in the diameter of the nanocomposite occurs during release and leads to the formation of fragmented CS.[49] Overall, our study confirms the release of dual drugs at lower and higher concentrations of Lyz in a sustained manner. Moreover, the delivery response could be customized by varying the drug concentration and Lyz content. Hence, the proposed strategy could work as a personalized therapy to treat glaucoma patients.

In comparison studies with commercially available formulations, namely, latoprost and Timolet, both formulations delivered the drugs in 2 h (LP) and 24 h (TM). Therefore, the developed drug nanocomposite could deliver the drug for a long time in response to naturally secreting ocular lysozyme by residing in the cornea due to mucoadhesiveness.

During drug release, it is expected that cleavage of the nanocomposite results in drug delivery. The surface FE-SEM image confirmed the cleavage of β-1,4 glycosidic linkages. The formation of cracked and uneven surfaces in the presence of Lyz suggests the release of dual drugs, while the drug nanocomposite appeared to be clear without any edges. Similar studies have reported the formation of sharp edges with an increase in the surface pore size upon Lyz treatment.[72] Liu *et al.* described the addition of Lyz to poly(D,L-lactic-*co*-glycolic acid) microspheres in CS scaffolds for tissue engineering applications, wherein the presence of enzyme leads to hydrolysis of the scaffold by forming an uneven surface, with cracked and discernible ragged edges.[73] Similarly, Kim *et al.* observed the degradation of CS hydrogel,[74] and Ahlen and co-workers reported the degradation of CS poly(acrylic acid) nanoparticles in the presence of an enzyme.[75,76]

To confirm the cleavage of β-1,4 glycosidic linkages in the presence of Lyz, a ^{1}H-NMR spectral study was carried out. The study showed the appearance of a peak at 3.8 ppm responsible for the formation of the –OH functional group after treatment with Lyz (dialysate), whereas the drug nanocomposite and Lyz-treated drug nanocomposite (retentate) did not show the same. The Lyz-treated drug nanocomposite did not demonstrate the –OH peak, possibly due to enzyme–substrate complex formation. Similar results were observed by Chou *et al.*, wherein carboxymethyl hexanoyl CS (CHC) was treated with Lyz to release insulin.[52] To confirm the structural similarity, ^{1}H-NMR spectroscopic studies were performed in which the data suggested that there were no significant changes to the chemical structure of the composite in the presence and absence of Lyz. Furthermore, it forms only fragmented low molecular weight CHC. In addition to this, Huang *et al.* reported that the formation of fragmented CS[49] could also be represented by emission spectroscopic studies; therefore, we used fluorescent GQDs to track the drug loading, delivery, and degradation of CS. Therefore, FE-SEM data and ^{1}H-NMR data confirm the cleavage of composite in the presence of Lyz.

To evaluate the *in vitro* toxicity of the developed drug nanocomposites, an MTT assay was conducted, and the drug nanocomposite and Lyz-treated drug nanocomposite showed >80% compatibility with HCE cells. The phenotype of the *in vitro* primary HCE cells has a better match with the *in vivo* tissues. Furthermore, these cultures of corneal cells will predict toxic reactions in the intact cornea *in vivo*.[53] Therefore, the toxicity of the nanocomposite was determined on HCE cells. Earlier studies reported more than 80% viability of cells in the presence of anti-glaucoma drug-loaded nanocomposite.[31,32] In addition, bright field imaging studies in the presence of 20, 60, and 100 μg mL^{−1} concentrations of the drug nanocomposite suggest the intact morphology of the HCE cells. Like the MTT analysis, AO/EB staining assay was performed using 20, 60, and 100 μg mL^{−1} concentrations of the drug

nanocomposite and Lyz-treated drug nanocomposite, which showed the compatibility of the nanocomposite by the appearance of green stained cells.

In addition to *in vitro* compatibility studies on HCE cells, the HET-CAM test also confirmed the non-irritancy of the developed nanocomposites and their precursors. The HET-CAM assay is considered a potential qualitative method to assess the ocular irritancy of chemicals. To investigate irritation, we have used a fertilized hen's egg, which is a laboratory-friendly and inexpensive method that gives an immense idea of ophthalmic irritation *in vivo*. Interestingly, as per the EU directive, if the material is not found to be corrosive or a severe irritant *in vitro*, *ex vivo* studies can be considered for evaluation in the case of ocular formulations and need not be extended for *in vivo* studies. Furthermore, histopathological staining of the CAM also suggests the growth of blood vessels, PC, SC, and TC. Hence, the study suggests the non-irritancy of the developed materials for ocular applications.

The molecular docking studies demonstrated the possible binding interaction between the polymer (CS) and drugs (LP and TM). LP showed a binding energy of -6.0 kcal mol^{-1} towards CS, while TM showed -5.9 kcal mol^{-1}. Generally, a low binding score depicts effective interactions of the drug with the polymer. Similar studies were reported by Dhanasekaran *et al.*, wherein the interactions of CS and chitin nanoparticles towards curcumin were determined by docking studies and a more stable structure was found by evaluating the number of hydrogen bonds and low binding energy.[77] Furthermore, LP–TM interactions showed a binding energy of -3.4 kcal mol^{-1}. Hence, the detailed molecular docking study showed the interactions of LP and TM towards the polymer chain and the formation of a stable structure.

In conclusion, we have developed a mucoadhesive drug nanocomposite for glaucoma drug delivery, which releases dual drugs in response to lysozyme. The drug loading was confirmed through fluorescence changes to GQDs by a simple PL spectroscopic study. XPS, UV-visible, FT-IR, and particle size analysis confirmed the successful formation of the drug nanocomposite. Molecular docking studies represent the interactions of the drug and CS. The prepared nanocomposite delivered 32.68% and 66.61% of LP and TM under the treatment of 1 mg mL^{-1} of lysozyme within 72 h of the study due to the cleavage of β-1,4 glycosidic linkages, which was confirmed by surface morphological FE-SEM, ^{1}H-NMR, and HPLC studies. In addition, *in vitro* cytotoxicity, live/dead staining, and bright field imaging assays proved good cell viability ($\geq$80%) upon treatment with 20–100 μg mL^{-1} of nanocomposite against HCE cell lines. *Ex vivo* studies indicate the non-irritancy of the composite for use in ophthalmic applications. Hence, by considering the secretion of lysozyme in the ocular region, the technology can be used to treat several ocular disorders and to manage mean diurnal IOP using medicated contact lenses. Besides, the work could also lead to personalized therapy for various disorders by considering the availability of lysozyme in saliva, lachrymal fluid, breast milk, intestines (secreted by Paneth cells), and stomach (present in mucinous granules and the rough endoplasmic reticulum).

The developed sustained dual drug deliverable systems could be employed for various ophthalmic and other disorders irrespective of the drug of interest. In addition, by considering the presence of lysozyme in the ophthalmic region, the drug nanocomposite could be utilized to develop soft contact lenses by initiating radical polymerization using poly(hydroxyethyl methacrylate) (pHEMA), thereby releasing the drug in a sustained manner. Furthermore, the enzyme-responsive drug release strategy could be explored in biomedical implants such as a microneedle and ocular inserts by employing nanocomposites. Apart from biomedical applications of the developed nanocomposites, they can also be employed for catalytic and electrochemical applications due to the reactive functional groups. Presently, our lab is focusing on the utilization of the nanocomposite for sensing applications, and in the future, it could be explored in various fields of research.

Conflicts of interest

The authors report no conflict of interest.

Acknowledgements

References

1 H. A. Quigley, Number of people with glaucoma worldwide, *Br. J. Ophthalmol.*, 1996, **80**(5), 389–393.

2 B. Thylefors and A. D. Négrel, The global impact of glaucoma, *Bull. W. H. O.*, 1994, **72**(3), 323–326.

3 C. W. McMonnies, Glaucoma history and risk factors, *J. Optom.*, 2017, **10**(2), 71–78.

4 K. Schwartz and D. Budenz, Current management of glaucoma, *Curr. Opin. Ophthalmol.*, 2004, **15**(2), 119–126.

5 A. Patel, K. Cholkar, V. Agrahari and A. K. Mitra, Ocular drug delivery systems: An overview, *World J. Pharmacol.*, 2013, **2**(2), 47–64.

6 N. Üstündağ Okur, E. Ş. Çağlar and P. I. Siafaka, Novel Ocular Drug Delivery Systems: An Update on Microemulsions, *J. Ocul. Pharmacol. Ther.*, 2020, **36**(6), 342–354.

7 B. N. Kumara, R. Shambhu and K. S. Prasad, Why chitosan could be apt candidate for glaucoma drug delivery - An overview, *Int. J. Biol. Macromol.*, 2021, **176**, 47–65.

8 J. Xu, Y. Ge, R. Bu, A. Zhang, S. Feng, J. Wang, *et al.*, Co-delivery of latanoprost and timolol from micelles-laden contact lenses for the treatment of glaucoma, *J. Controlled Release*, 2019, **305**, 18–28.

9 B. N. Kumara, K. Velmurugan, M. V. Ghate, R. Shambhu, J. Nirmal and K. S. Prasad, A promising "single" and "dual" drug-nanocomposite enriched contact lens for the management of glaucoma in response to the lacriaml fluid enzyme, *J. Mater. Chem. B*, 2024, **12**(9), 2394–2412.

10 V. Kailasam, B. N. Kumara, K. S. Prasad and J. Nirmal, Combination of self-assembling system and N,O-carboxymethyl chitosan improves ocular residence of anti-glaucoma drug, *Eur. J. Pharm. Biopharm.*, 2024, **197**, 114208.

11 V. Agrahari, A. Mandal, V. Agrahari, H. M. Trinh, M. Joseph, A. Ray, *et al.*, A comprehensive insight on ocular pharmacokinetics, *Drug Delivery Transl. Res.*, 2016, **6**(6), 735–754.

12 E. Lavik, M. H. Kuehn and Y. H. Kwon, Novel drug delivery systems for glaucoma, *Eye*, 2011, **25**(5), 578–586.

13 R. B. Singh, P. Ichhpujani, S. Thakur and S. Jindal, Promising therapeutic drug delivery systems for glaucoma: a comprehensive review, *Ther. Adv. Ophthalmol.*, 2020, **12**, 2515841420905740.

14 M. M. Allyn, R. H. Luo, E. B. Hellwarth and K. E. Swindle-Reilly, Considerations for Polymers Used in Ocular Drug Delivery, *Front. Med.*, 2022, **8**, 787644.

15 L. Wang, Y. Y. Jiang and N. Lin, Promise of latanoprost and timolol loaded combinatorial nanosheet for therapeutic applications in glaucoma, *J. King Saud Univ., Sci.*, 2020, **32**(1), 1042–1047.

16 A. F. Pereira-da-Mota, C. M. Phan, A. Concheiro, L. Jones and C. Alvarez-Lorenzo, Testing drug release from medicated contact lenses: The missing link to predict in vivo performance, *J. Controlled Release*, 2022, **343**, 672–702.

17 R. Asasutjarit, S. Thanasanchokpibull, A. Fuongfuchat and S. Veeranondha, Optimization and evaluation of thermoresponsive diclofenac sodium ophthalmic in situ gels, *Int. J. Pharm.*, 2011, **411**(1), 128–135.

18 M. Rajaei, H. Rashedi, F. Yazdian, M. Navaei-Nigjeh, A. Rahdar and A. M. Díez-Pascual, Chitosan/agarose/graphene oxide nanohydrogel as drug delivery system of 5-fluorouracil in breast cancer therapy, *J. Drug Delivery Sci. Technol.*, 2023, **82**, 104307.

19 H. Abdouss, M. Pourmadadi, P. Zahedi, M. Abdouss, F. Yazdian, A. Rahdar, *et al.*, Green synthesis of chitosan/polyacrylic acid/graphitic carbon nitride nanocarrier as a potential pH-sensitive system for curcumin delivery to MCF-7 breast cancer cells, *Int. J. Biol. Macromol.*, 2023, **242**, 125134.

20 M. H. Karami, M. Pourmadadi, M. Abdouss, M. R. Kalaee, O. Moradi, A. Rahdar, *et al.*, Novel chitosan/γ-alumina/carbon quantum dot hydrogel nanocarrier for targeted drug delivery, *Int. J. Biol. Macromol.*, 2023, **251**, 126280.

21 B. N. Kumara, N. G. Gurudatt and K. S. Prasad, Carboxymethyl-hexanoyl chitosan: A promising candidate for hydrophobic and hydrophilic drug delivery, *Carbohydr. Polym. Technol. Appl.*, 2023, **6**, 100401.

22 F. Rezaei Abbas Abad, M. Pourmadadi, M. Abdouss, R. Behzadmehr, A. Rahdar and S. Pandey, Chitosan-Carbon nanotube Composite: An approach for controlled release of Quercetin, Modified with carboxymethyl Cellulose, for potential Anti-Cancer therapy, *Inorg. Chem. Commun.*, 2023, **158**, 111621.

23 R. M. Gilhotra and D. N. Mishra, Alginate-chitosan film for ocular drug delivery: effect of surface cross-linking on film properties and characterization, *Pharmazie*, 2008, **63**(8), 576–579.

24 R. Alford, H. M. Simpson, J. Duberman, G. C. Hill, M. Ogawa, C. Regino, *et al.*, Toxicity of Organic Fluorophores Used in Molecular Imaging: Literature Review, *Mol. Imaging*, 2009, **8**(6), 341–354.

25 E. C. Jensen, Use of fluorescent probes: their effect on cell biology and limitations, *Anat. Rec.*, 2012, **295**(12), 2031–2036.

26 Z. H. Li, J. Peng and H. L. Chen, Bioconjugated quantum dots as fluorescent probes for biomedical imaging, *J. Nanosci. Nanotechnol.*, 2011, **11**(9), 7521–7536.

27 K. O'goshi and J. Serup, Safety of sodium fluorescein for in vivo study of skin, *Sking Res. Technol.*, 2006, **12**(3), 155–161.

28 B. N. Kumara, P. Kalimuthu and K. S. Prasad, Synthesis, properties and potential applications of photoluminescent carbon nanoparticles: A review, *Anal. Chim. Acta*, 2023, **1268**, 341430.

29 S. Zhu, N. Zhou, Z. Hao, S. Maharjan, X. Zhao, Y. Song, *et al.*, Photoluminescent graphene quantum dots for in vitro and in vivo bioimaging using long wavelength emission, *RSC Adv.*, 2015, **5**(49), 39399–39403.

30 M. C. Biswas, M. T. Islam, P. K. Nandy and M. M. Hossain, Graphene Quantum Dots (GQDs) for Bioimaging and Drug Delivery Applications: A Review, *ACS Mater. Lett.*, 2021, **3**(6), 889–911.

31 B. N. Kumara, R. Shambhu, Y. B. Shim, J. Nirmal and K. S. Prasad, Development of mucoadhesive Timolol loaded chitosan-nanocomposite to treat glaucoma, *Int. J. Biol. Macromol.*, 2023, **253**, 126917.

32 B. N. Kumara, R. Shambhu, A. Prabhu and K. S. Prasad, Novel chitosan - graphene quantum dots composite for therapeutic delivery and tracking through enzymatic stimuli response, *Carbohydr. Polym.*, 2022, **289**, 119426.

33 M. Tighsazzadeh, J. C. Mitchell and J. S. Boateng, Development and evaluation of performance characteristics of timolol-loaded composite ocular films as potential delivery platforms for treatment of glaucoma, *Int. J. Pharm.*, 2019, **566**, 111–125.

34 R. Ilka, M. Mohseni, M. Kianirad, M. Naseripour, K. Ashtari and B. Mehravi, Nanogel-based natural polymers as smart carriers for the controlled delivery of Timolol Maleate through the cornea for glaucoma, *Int. J. Biol. Macromol.*, 2018, **109**, 955–962.

35 F. A. P. de Sá, S. F. Taveira, G. M. Gelfuso, E. M. Lima and T. Gratieri, Liposomal voriconazole (VOR) formulation for improved ocular delivery, *Colloids Surf., B*, 2015, **133**, 331–338.

36 G. Tan, S. Yu, H. Pan, J. Li, D. Liu, K. Yuan, *et al.*, Bioadhesive chitosan-loaded liposomes: A more efficient and higher permeable ocular delivery platform for timolol maleate, *Int. J. Biol. Macromol.*, 2017, **94**, 355–363.

37 T. Mosmann, Rapid colorimetric assay for cellular growth and survival: application to proliferation and cytotoxicity assays, *J. Immunol. Methods*, 1983, **65**(1–2), 55–63.

38 H. S. Vethakanraj, T. A. Babu, G. B. Sudarsanan, P. K. Duraisamy and S. Ashok Kumar, Targeting ceramide metabolic pathway induces apoptosis in human breast cancer cell lines, *Biochem. Biophys. Res. Commun.*, 2015, **464**(3), 833–839.

39 H. Abdelkader, B. Pierscionek, M. Carew, Z. Wu and R. G. Alany, Critical appraisal of alternative irritation models: three decades of testing ophthalmic pharmaceuticals, *Br. Med. Bull.*, 2015, **113**(1), 59–71.

40 N. Dilbaghi, H. Kaur, M. Ahuja and S. Kumar, Evaluation of tropicamide-loaded tamarind seed xyloglucan nanoaggregates for ophthalmic delivery, *Carbohydr. Polym.*, 2013, **94**(1), 286–291.

41 J. Hao, X. Wang, Y. Bi, Y. Teng, J. Wang, F. Li, *et al.*, Fabrication of a composite system combining solid lipid nanoparticles and thermosensitive hydrogel for challenging ophthalmic drug delivery, *Colloids Surf., B*, 2014, **114**, 111–120.

42 R. Zhao, J. Li, J. Wang, Z. Yin, Y. Zhu and W. Liu, Development of Timolol-Loaded Galactosylated Chitosan Nanoparticles and Evaluation of Their Potential for Ocular Drug Delivery, *AAPS PharmSciTech*, 2017, **18**(4), 997–1008.

43 X. Y. Meng, H. X. Zhang, M. Mezei and M. Cui, Molecular docking: a powerful approach for structure-based drug discovery, *Curr. Comput.-Aided Drug Des.*, 2011, **7**(2), 146–157.

44 O. Trott and A. J. Olson, AutoDock Vina: improving the speed and accuracy of docking with a new scoring function, efficient optimization and multithreading, *J. Comput. Chem.*, 2010, **31**(2), 455–461.

45 K. Thoma and I. Ziegler, Simultaneous quantification of released succinic acid and a weakly basic drug compound in dissolution media, *Eur. J. Pharm. Biopharm.*, 1998, **46**(2), 183–190.

46 T. Wen, F. Qu, N. B. Li and H. Q. Luo, A facile, sensitive, and rapid spectrophotometric method for copper(II) ion detection in aqueous media using polyethyleneimine, *Arabian J. Chem.*, 2017, **10**, S1680–S1685.

47 Y. A. El-Feky, D. A. Mostafa, M. M. Al-Sawahli, R. F. A. El-Telbany, S. Zakaria, A. M. Fayez, *et al.*, Reduction of intraocular pressure using timolol orally dissolving strips in the treatment of induced primary open-angle glaucoma in rabbits, *J. Pharm. Pharmacol.*, 2020, **72**(5), 682–698.

48 S. Gorantla, V. K. Rapalli, T. Waghule, P. P. Singh, S. K. Dubey, R. N. Saha, *et al.*, Nanocarriers for ocular drug delivery: current status and translational opportunity, *RSC Adv.*, 2020, **10**(46), 27835–27855.

49 H. Huang, F. Liu, S. Chen, Q. Zhao, B. Liao, Y. Long, *et al.*, Enhanced fluorescence of chitosan based on size change of micelles and application to directly selective detecting Fe3+ in humanserum, *Biosens. Bioelectron.*, 2013, **42**, 539–544.

50 S. K. L. Levengood and M. Zhang, Chitosan-based scaffolds for bone tissue engineering, *J. Mater. Chem. B*, 2014, **2**(21), 3161–3184.

51 G. V. Nájera-Romero, M. Yar and I. U. Rehman, Heparinized chitosan/hydroxyapatite scaffolds stimulate angiogenesis, *Funct. Compos. Mater.*, 2020, **1**(1), 9.

52 H. S. Chou, M. Larsson, M. H. Hsiao, Y. C. Chen, M. Röding, M. Nydén, *et al.*, Injectable insulin-lysozyme-loaded nanogels with enzymatically-controlled degradation and release for basal insulin treatment: In vitro characterization and in vivo observation, *J. Controlled Release*, 2016, **224**, 33–42.

53 S. Rönkkö, K. S. Vellonen, K. Järvinen, E. Toropainen and A. Urtti, Human corneal cell culture models for drug toxicity studies, *Drug Delivery Transl. Res.*, 2016, **6**(6), 660–675.

54 P. Yadav, A. Bandyopadhyay, A. Chakraborty and K. Sarkar, Enhancement of anticancer activity and drug delivery of chitosan-curcumin nanoparticle via molecular docking and simulation analysis, *Carbohydr. Polym.*, 2018, **182**, 188–198.

55 J. Dong, K. Wang, L. Sun, B. Sun, M. Yang, H. Chen, *et al.*, Application of graphene quantum dots for simultaneous fluorescence imaging and tumor-targeted drug delivery, *Sens. Actuators, B*, 2018, **256**, 616–623.

56 H. Manisha, M. Velayudham, B. N. Kumara, M. H. Naveen, Y. B. Shim and K. S. Prasad, Revelation of fluorophore impurities among biocompatible blue fluorescent carbon nanodots derived from Hemigraphis alternata plant and bioimaging, *Carbon Lett.*, 2023, **33**(3), 931–946.

57 I. Srivastava, P. Moitra, D. Sar, K. Wang, M. Alafeef, J. Scott, *et al.*, Luminescence switching in polymerically confined carbon nanoparticles triggered by UV-light, *Nanoscale*, 2021, **13**(38), 16288–16295.

58 S. K. Misra, I. Srivastava, I. Tripathi, E. Daza, F. Ostadhossein and D. Pan, Macromolecularly "Caged" Carbon Nanoparticles for Intracellular Trafficking via Switchable Photoluminescence, *J. Am. Chem. Soc.*, 2017, **139**(5), 1746–1749.

59 L. D. Field, S. A. Walper, K. Susumu, G. Lasarte-Aragones, E. Oh, I. L. Medintz, *et al.*, A Quantum Dot-Protein Bioconjugate That Provides for Extracellular Control of Intracellular Drug Release, *Bioconjugate Chem.*, 2018, **29**(7), 2455–2467.

60 H. Li, C. Sun, R. Vijayaraghavan, F. Zhou, X. Zhang and D. R. MacFarlane, Long lifetime photoluminescence in N, S co-doped carbon quantum dots from an ionic liquid and their applications in ultrasensitive detection of pesticides, *Carbon*, 2016, **104**, 33–39.

61 R. Sinha, A. Chatterjee and P. Purkayastha, Graphene Quantum Dot Assisted Translocation of Daunomycin through an Ordered Lipid Membrane: A Study by

Fluorescence Lifetime Imaging Microscopy and Resonance Energy Transfer, *J. Phys. Chem. B*, 2022, **126**(6), 1232–1241.

62 W. Hu and X. Yuan, Facile Hydrothermal Synthesis of SnO₂ Nanospheres as Photocatalysts, *J. Nanomater.*, 2017, **2017**, e6976203.

63 S. Kumar and J. Koh, Physiochemical, Optical and Biological Activity of Chitosan-Chromone Derivative for Biomedical Applications, *Int. J. Mol. Sci.*, 2012, **13**(5), 6102–6116.

64 S. B. Aziz, R. T. Abdulwahid, M. A. Rasheed, O. G. H. Abdullah and H. M. Ahmed, Polymer Blending as a Novel Approach for Tuning the SPR Peaks of Silver Nanoparticles, *Polymers*, 2017, **9**(10), 486.

65 C. Bochaton, R. Boistel and L. Charles, X-ray microtomography provides first data about the feeding behaviour of an endangered lizard, the Montserrat galliwasp (Diploglossus montisserrati), *R. Soc. Open Sci.*, 2015, **2**(12), 150461.

66 M. A. Dubey, Investigation of hydrogel membranes containing a combination of timolol maleate and brimonidine tartrate for ocular delivery, *Asian J. Pharm.*, 2014, **8**(4), 259–270.

67 A. M. L. Rubenicia, L. D. P. Cubillan, V. A. D. P. Sicam, A. P. G. Macabeo, O. B. Villaflores and A. L. Castillo, Intraocular Pressure Reduction Effect of 0.005% Latanoprost Eye Drops in a Hyaluronic Acid-Chitosan Nanoparticle Drug Delivery System in Albino Rabbits, *Transl. Vision Sci. Technol.*, 2021, **10**(4), 2.

68 A. Zamboulis, S. Nanaki, G. Michailidou, I. Koumentakou, M. Lazaridou, N. M. Ainali, *et al.*, Chitosan and its Derivatives for Ocular Delivery Formulations: Recent Advances and Developments, *Polymers*, 2020, **12**(7), 1519.

69 I. Aranaz, A. R. Alcántara, M. C. Civera, C. Arias, B. Elorza, A. Heras Caballero, *et al.*, Chitosan: An Overview of Its Properties and Applications, *Polymers*, 2021, **13**(19), 3256.

70 N. Nwe, T. Furuike and H. Tamura, The Mechanical and Biological Properties of Chitosan Scaffolds for Tissue Regeneration Templates Are Significantly Enhanced by Chitosan from Gongronella butleri, *Materials*, 2009, **2**(2), 374–398.

71 P. Velos, P. M. Cherry and D. Miller, An improved method for measuring human tear lysozyme concentration, *Arch. Ophthalmol.*, 1985, **103**(1), 31–33.

72 Z. Ma, C. Yang, W. Song, Q. Wang, J. Kjems and S. Gao, Chitosan Hydrogel as siRNA vector for prolonged gene silencing, *J. Nanobiotechnol.*, 2014, **12**(1), 23.

73 Y. Liu, C. Zhou and Y. Sun, A biomimetic strategy for controllable degradation of chitosan scaffolds, *J. Mater. Res.*, 2012, **27**(14), 1859–1868.

74 S. Kim, Z. K. Cui, B. Koo, J. Zheng, T. Aghaloo and M. Lee, Chitosan-Lysozyme Conjugates for Enzyme-Triggered Hydrogel Degradation in Tissue Engineering Applications, *ACS Appl. Mater. Interfaces*, 2018, **10**(48), 41138–41145.

75 M. Åhlén, G. K. Tummala and A. Mihranyan, Nanoparticle-loaded hydrogels as a pathway for enzyme-triggered drug release in ophthalmic applications, *Int. J. Pharm.*, 2018, **536**(1), 73–81.

76 A. Lončarević, M. Ivanković and A. Rogina, Lysozyme-Induced Degradation of Chitosan: The Characterisation of Degraded Chitosan Scaffolds, *J. Tissue Repair Regener.*, 2017, **1**(1), 12–22.

77 S. Dhanasekaran, P. Rameshthangam, S. Venkatesan, S. K. Singh and S. R. Vijayan, In Vitro and In Silico Studies of Chitin and Chitosan Based Nanocarriers for Curcumin and Insulin Delivery, *J. Polym. Environ.*, 2018, **26**(10), 4095–4113.